Chinese Chemical Letters 37 (2026) 110860

Contents lists available at ScienceDirect

Chinese Chemical Letters

journal homepage: www.elsevier.com/locate/cclet

Porous carbon derived from biomass-based polymers: Innovative applications in supercapacitors

Qiqi Lv[a], Zhiwei Tian[a], Weijun Li[b,*], Gaigai Duan[a], Xiaoshuai Han[a], Chunmei Zhang[c,*], Shuijian He[a], Haimei Mao[d,*], Chunxin Ma[d], Shaohua Jiang[a,*]

[a] Jiangsu Co-Innovation Center of Efficient Processing and Utilization of Forest Resources, International Innovation Center for Forest Chemicals and Materials, College of Materials Science and Engineering, Nanjing Forestry University, Nanjing 210037, China
[b] Institute of Micro/Nano Materials and Devices, Ningbo University of Technology, Ningbo 315211, China
[c] Institute of Materials Science and Devices, School of Materials Science and Engineering, Suzhou University of Science and Technology, Suzhou 215009, China
[d] Key Laboratory of Quality Safe Evaluation and Research of Degradable Material, State Administration for Market Regulation, Hainan Academy of Inspection and Testing, Haikou 570203, China

ARTICLE INFO

Article history:
Received 15 December 2024
Revised 11 January 2025
Accepted 14 January 2025
Available online 16 January 2025

Keywords:
Bio-based polymers
Porous carbon
Activation
Heteroatom doping
Supercapacitors

ABSTRACT

In the context of the continuously increasing energy demand, the ongoing advancement of innovative energy storage technologies is regarded as an important strategy to alleviate the energy crisis. Among various energy storage technologies, supercapacitors (SCs) demonstrate significant potential in the future energy storage sector due to their exceptional high-power density and long cycle life. As the core component of SCs, the choice of electrode materials is crucial to their performance, with carbon materials being favored for their excellent electrical conductivity and large specific surface area. In particular, porous carbon materials derived from biomass-based polymers have become a research hotspot due to their unique advantages. Through chemical modification and high-temperature carbonization, these materials can form more stable and optimized porous structures, significantly enhancing their electrochemical performance while meeting environmental protection requirements, thereby highlighting their superiority as electrode materials. This article aims to review the sources, production, and applications of carbon materials derived from biomass-based polymers. We have deeply summarized the preparation and activation methods of carbon from different biomass-based polymer sources. In addition, a comprehensive analysis and systematic comparison of novel modification techniques, such as heteroatom doping, copolymerization, and the incorporation of nanomaterials, were performed to enhance the performance of SCs. Finally, according to the technical challenges to be solved, the goal of large-scale development of biomass-based polymer-derived porous carbon in the field of energy storage is proposed, which is crucial for coping with the global energy crisis and reducing environmental impact.

© 2026 Published by Elsevier B.V. on behalf of Chinese Chemical Society and Institute of Materia Medica, Chinese Academy of Medical Sciences.

1. Introduction

In recent years, global climate change has intensified, with the speed of global warming surpassing expectations. This change not only affects biodiversity, glacier melting, and sea level rise, but it may also have profound effects on the politics and economies of various countries [1–5]. The main cause of global warming is the overuse of fossil fuels, especially coal, oil and natural gas. The greenhouse gases released by these fuels during combustion, such as carbon dioxide (CO_2), methane (CH_4) and nitrous oxide (N_2O), contribute to climate change. Therefore, the exploration of clean and sustainable energy sources, such as solar energy, wind energy, and bioenergy, as well as the pursuit of efficient energy storage technologies, has become an urgent task at present [6–9]. Among various energy storage technologies, electrochemical energy storage technology is regarded as the most practical, reliable, and efficient, such as such as Li-ion battery [10], ammonium-ion batteries [11], hybrid battery [12], Li-S batteries [13], Zn-ion batteries [14], microbial fuel cell [15], supercapacitor [16], zinc-ion hybrid supercapacitors [17]. Compared to traditional energy storage methods,

* Corresponding authors.
E-mail addresses: lwj1214417@163.com (W. Li), cmzhang@usts.edu.cn (C. Zhang), mcmhm@163.com (H. Mao), shaohua.jiang@njfu.edu.cn (S. Jiang).

https://doi.org/10.1016/j.cclet.2025.110860
1001-8417/© 2026 Published by Elsevier B.V. on behalf of Chinese Chemical Society and Institute of Materia Medica, Chinese Academy of Medical Sciences.

electrochemical energy storage technology stores and releases electrical energy in the form of chemical energy. SCs have attracted much attention due to their advantages of fast charge and discharge speed, long cycle life, high power density, low environmental pollution and fast response speed. The performance of SCs is closely related to the electrode materials, electrolytes, and binders, with the electrode materials often being the key factor influencing their performance. Commonly used electrode materials include carbon materials, metal oxides, and conductive polymers, among others [18–22].

Carbon-based electrode materials present several advantages, including low cost, high conductivity, large specific surface area, controllable pore size, and excellent stability. With the increasing demand for development and the urgency of human survival, there is an urgent need for renewable energy to replace fossil fuels [23,24]. In the current energy field, biomass-based polymers have received extensive attention due to their biocompatibility, sustainability and accessibility. More importantly, the carbon derived from biomass-based polymers possesses good biodegradability and environmental friendliness, aligning with the principles of sustainable development and reducing dependence on traditional petroleum-based carbon materials [25–27]. Compared to traditional carbon materials, the pyrolysis and carbonization processes of biomass-based polymers are more controllable. The structure of the final carbon materials can be optimized by adjusting factors such as reaction time and atmosphere. In addition, porous carbon from biomass-based polymers has a larger surface area, which helps charge storage, and can increase ion transport rate in the process of regulating biomass-based polymer precursors and carbonization conditions. Due to the selection of precursors and the structural characteristics after carbonization, porous carbon derived from biomass-based polymers typically exhibits higher electrical conductivity. The design of biomass-based polymers can also achieve finer regulation at the microscopic level through the introduction of surface functional groups and chemical modification methods [28–32].

Carbon materials derived from biomass-based polymers are promising materials for SCs. Nonetheless, few reviews emphasize the applications of porous carbon derived from biomass-based polymers in SCs. Therefore, there is still a need for a comprehensive overview of the applications of porous carbon derived from biomass-based polymers in SCs. This article briefly summarizes and discusses the latest advances in the application of biomass polymers in SCs. Moreover, the review also emphasizes the correlation analysis of various porous carbons derived from biomass-based polymers in energy storage for SCs. Additionally, the review also emphasizes strategies for enhancing the performance of various biomass-derived porous carbons in SCs through novel modification methods. Finally, this study objectively discusses the limitations of biomass-based polymers in achieving green and sustainable energy storage, while also proposing potential directions for future research (Fig. 1).

2. Sources of bio-based polymers

Biomass refers to organic materials derived from living organisms and serves as a natural and abundant source of renewable energy and raw materials. It primarily includes wood, crops, animal manure, and various forms of waste [33–39]. Biomass-based polymers are materials synthesized from biomass raw materials through chemical or biosynthetic pathways [40]. These polymers exhibit both biocompatibility and biodegradability [41]. Based on the types of polymers, biomass-based polymers can be broadly categorized into two categories: Natural biopolymers and synthetic biopolymers.

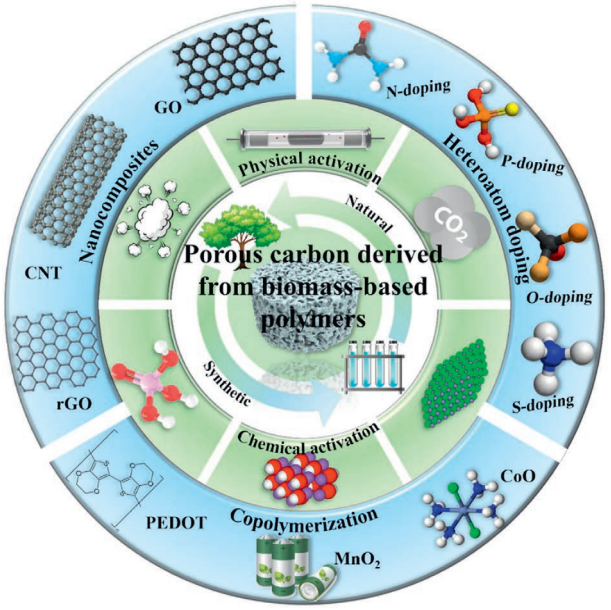


Fig. 1. The design and properties of porous carbon derived from biomass-based polymers are discussed to promote the development of supercapacitors. Reproduced with permission [8]. Copyright 2024, The Authors. Reproduced with permission [4]. Copyright 2024, Elsevier B.V. Reproduced with permission [31]. Copyright 2024, American Chemical Society. Reproduced with permission [32]. Copyright 2020, Elsevier Ltd.

2.1. Natural biopolymers

2.1.1. Plant-based polymers

Plant-based polymers primarily consist of cellulose, hemicellulose, and lignin. Consequently, their structure and composition usually depend on the type of plant. The primary advantages of plant-based polymers are their abundance, biodegradability, and environmental sustainability. In addition, these polymers contain a large amount of carbon, which plays a vital role in the subsequent preparation of biomass-based carbon materials. According to their origin and structure, plant-based polymers can be divided into the following categories: cellulose-based, lignin-based, and starch-based, as well as plant-derived polymers, which include natural resins and gums.

2.1.1.1. Cellulose and its derivatives. Cellulose is the most abundant and widely distributed biomass resource in nature, mainly derived from plant fibers (such as wood, hemp, bamboo) [42–47]. It is a carbohydrate polymer with the chemical formula $(C_6H_{10}O_5)$ n, where the value of (n) typically ranges from 1000 to 30,000, and can reach up to 100,000, depending on the type of plant [48–50]. From a molecular perspective, cellulose molecules are linear polymers composed of glucose as the basic unit. Each glucose pyran unit contains one primary hydroxyl group (C_6-OH) and two secondary hydroxyl groups (C_2-OH and C_3-OH). These units consist of two simple carbohydrates, which are D-glucose rings linked by $\beta-1,4$-glycosidic bonds (Fig. 2a). The presence of oxygen atoms in the closed ring of D-glucose promotes the formation of intermolecular hydrogen bonds, which is also key to the stability of the cellulose molecular structure. Cellulose microfibrils are aggregated into highly ordered regions (crystalline regions) and disordered regions (amorphous regions). In the crystalline regions of cellulose, the orderly arrangement of molecular chains allows the hydroxyl groups on both sides to form hydrogen bonds with the hydroxyl groups on adjacent chains, thereby creating a lattice structure. However, in the disordered regions of the cellulose molecular chains, there are relatively large gaps between the chains, which results in a

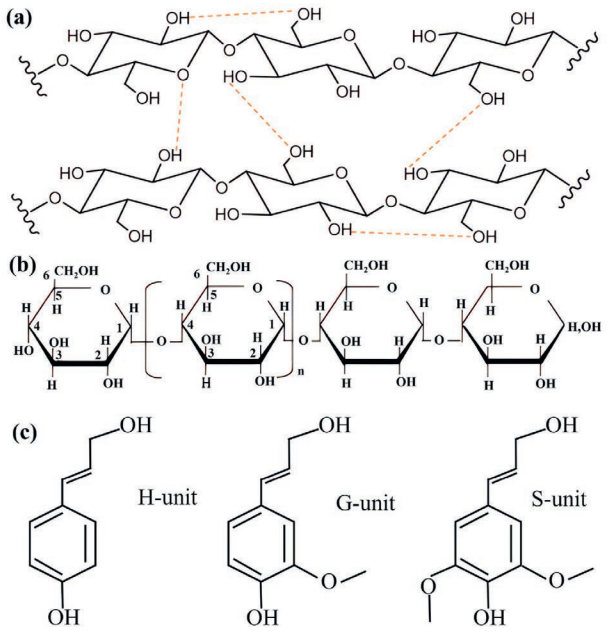


Fig. 2. Structure of plant-based polymers. (a) The structure of plant-based polymers. Reproduced with permission [75]. Copyright 2024, Elsevier Ltd. (b) The structure of starch. Reproduced with permission [73]. Copyright 2003, Elsevier Science Ltd. (c) Microstructures of different types of lignin. Reproduced with permission [74]. Copyright 2024, American Chemical Society.

decrease in intermolecular hydrogen bonds, leading to the formation of an amorphous region [51,52]. According to the crystalline structure of cellulose, it can be divided into four forms: Type I, type II, type III, and type IV [53–55]. Among these, cellulose type I is sometimes referred to as natural cellulose. Due to its structural stability, excellent flexibility, and good porosity, cellulose has been widely applied in SCs. In addition, cellulose is a white, odorless powder that is insoluble in water and most organic solvents. However, it can be dissolved in ammonia solutions containing copper oxide, concentrated solutions of ammonium chloride, saturated solutions of sodium thiocyanate, and other salts.

In addition, cellulose derivatives are generated through the esterification or etherification reactions of hydroxyl groups in cellulose with chemical reagents. According to the structural characteristics, cellulose derivatives can be divided into cellulose esters, cellulose ethers and cellulose ester ethers. At the same time, nanocellulose is also a very promising material. Nanocellulose can be classified into cellulose nanofibers (CNFs), cellulose nanocrystals (CNCs), and bacterial cellulose (BC) based on appearance and preparation methods [56–58]. Cellulose nanofiber is a kind of long fibrous nanocellulose with a diameter of 1–100 nm and a length ranging from 100 nm to several microns [59–61]. Cellulose nanocrystals are rod-shaped cellulose crystals, typically extracted from various cellulose materials through acid hydrolysis. Their widths range from 5 nm to 70 nm, while their lengths vary from 100 nm to several micrometers [62–64]. Compared with CNCs and CNFs, BC has higher chemical purity and unique nanostructures [65]. The sustainability and environmental friendliness of nanocellulose make it a promising candidate for cellulose-based energy storage devices in future electronic products.

2.1.1.2. Starch. Starch serves as a significant source of complex carbohydrates in the food chain, second only to cellulose. It is a polysaccharide composed of numerous glucose units linked by glycosidic bonds. Amylose and amylopectin are the main components of starch. Amylose is a linear polymer composed of glucose molecules connected by $\alpha-1,4$-glycosidic bonds, accounting for about 20 %–30 % of starch molecules. It exhibits a helical structure, which contributes to thickening and gelation when heated with water. Relatively speaking, amylopectin accounts for about 70 %–80 % of starch molecules. It is a branched polymer with $\alpha-1,4$-and $\alpha-1,6$-glycosidic bonds [66–68]. It has a branched structure and can enhance the viscosity and texture of starch solution (Fig. 2b). Starch contains a large number of hydroxyl groups, which makes it have high hydrophilicity. Furthermore, starch can be modified through esterification and etherification to enhance its properties and broaden its applications across various fields. Starch is primarily sourced from corn, rice, wheat, sorghum, cassava, potato, sweet potato, and taro [69–72]. Starch derived from different sources typically exhibits variations in composition and structural characteristics, leading to differences in their physical and chemical properties, including thermal behavior, solubility, swelling, hydrolysis, and degradation. Additionally, starch-based materials are extensively utilized in food production, papermaking, textiles, adhesives, carbon materials, and pharmaceuticals.

2.1.1.3. Lignin. Lignin is the most abundant aromatic natural polymer on earth, accounting for about 15 %–30 % of natural organisms. In natural plant biomass, lignin, cellulose and hemicellulose are cross-linked. Lignin fills the gap between cellulose and plate cellulose and acts as a binder. Lignin usually exists in the outer layer of plants and binds to polysaccharides [73–75]. The chemical structure of lignin is complex and there is no strict fixed structure, and its structure will vary according to the source of lignin and the extraction method. Typically, lignin is a three-dimensional aromatic molecule formed by the interconnection of three phenylpropyl alkyl units through different ether bonds and carbon-carbon bonds. The three monomeric alcohols derived from the phenylpropane structural unit are p-coumaryl alcohol, coniferyl alcohol, and sinapyl alcohol. Correspondingly, these lead to three types of lignin monomers: *p*-Hydroxyphenyl lignin (H-lignin), syringyl lignin (S-lignin), and guaiacyl lignin (G-lignin). The binding of different structural units usually occurs at the C-O bond and the C-C bond, forming β-O-4, β-β, $\beta-1,4$-O-5 and 5–5 connections (Fig. 2c). Lignin is abundant in functional groups, including hydroxyl (-OH), carboxyl (-COOH), phenolic (-Ph-OH), and carbonyl (-C=O) groups, so its active groups are chemically unstable [76–79]. These reactions facilitate the conversion of lignin molecules into functional materials. Furthermore, lignin can be extracted using various industrial and laboratory methods. The lignin obtained in the experiment comprised milled wood lignin, lignin from cellulose-degrading enzymes, and enzymatically mild acid-hydrolyzed lignin. Industrial lignin derivatives predominantly originate from by-products of the paper industry. Specifically, lignin derivatives produced during the pulping process include lignosulfonate (LS), alkali lignin (AL), and Kraft lignin (KL) with lignosulfonate representing the largest share of global lignin production [80–83]. In addition, lignin is the only phenolic polymer in plant resources, characterized by its hydrophobicity and stability. It contains a large number of oxygen-containing functional groups, such as methoxy, hydroxyl, carboxyl, and ether groups, which endow lignin with many attractive energy storage properties.

2.1.2. Animal-based polymers

In our country, over one million tons of meat by-products, such as animal bones and hides, are often discarded as waste, primarily originating from the food industry and our daily lives [84–86]. Biomass materials of animal origin mainly come from the renewable and shed parts of the animal body, although some are not usable (Fig. 3a). Generally, animal skin is primarily composed of proteins, water, lipids, and carbohydrates. In addition to the common elements carbon (C), hydrogen (H), and oxygen (O), animal tissues also contain other elements such as nitrogen (N), phosphorus (P),



Fig. 3. Structure of animal-based polymers. (a) Animal-derived proteins. Reproduced with permission [38]. Copyright 2022, IOP Publishing Ltd. (b) The molecular structure of keratin. Reproduced with permission [98]. Copyright 2024, Springer Nature. (c) Animal-derived chitosan. Reproduced with permission [38]. Copyright 2022, IOP Publishing Ltd. (d) The structure of chitin. Reproduced with permission [103]. Copyright 2023, Elsevier B.V.

and sulfur (S). Additionally, animal bodies contain ribonucleic acid (RNA), which is a biomolecule involved in the transmission of genetic information and the synthesis of proteins. According to the source and structure, animal-derived biopolymers can be divided into two categories: protein-based, including silk, collagen, keratin, *etc*., and chitosan-based polymers.

2.1.2.1. Protein. Silk is one of the oldest protein-based biopolymers utilized by humans, possessing a variety of functions. Silk are natural fibers produced by silkworms and spiders, and they have been widely studied due to their high yield characteristics. Silk is composed of primary polypeptide chains made up of amino acid monomers, containing 70 % to 80 % fibroin (silk protein) and 20 % to 30 % sericin (gum protein), with sericin wrapping around the fibroin protein [87–90]. Fibroin exhibits excellent properties such as toughness, tensile strength, biocompatibility, and biodegradability.

Collagen is a protein-based polymer primarily found in the extracellular matrix of all multicellular organisms, serving as a major insoluble fibrous protein. It can be obtained from various mammals (such as pigs and goats) and non-mammals (such as fish and amphibians), and it is a major component of bones, blood vessels, tendons, and skin [91–94]. Collagen is a highly ordered protein primarily composed of three polypeptide chains that intertwine to form a triple helix structure. T This structure gives collagen a strong mechanical strength and toughness, while rich in various atoms, such as oxygen, nitrogen, especially carbon.

Keratin is a versatile biopolymer that provides an outer covering and strength to the bodies and muscles of most mammals. It is primarily a major component of hair, wool, feathers, and nails. Keratin is rich in cysteine, which allows it to form many disulfide bonds, imparting certain stability and compressive strength. It typically aggregates in helical or sheet-like forms to form robust fibers. Keratin can be classified into α-keratin and β-keratin (Fig. 3b) [95–98]. α-Keratin is mainly found in the hair, skin, and nails of mammals, exhibiting good toughness and stretchability. On the other hand, β-keratin is mainly present in the feathers of birds, the skin and horns of reptiles, and is usually harder and wear-resistant. Keratin is important for energy applications because the presence of nitrogen atoms enhances the transport of carbon-activated ions.

2.1.2.2. Chitosan. Chitosan is abundant in nature and is a widely distributed biopolymer found in the exoskeletons of crustaceans, shellfish, and fungi (Fig. 3c) [99,100]. The basic unit of chitosan is composed of two subunits of d-glucosamine, and *n*-acetyl-d-glucosamine is linearly linked by 1,4-glycosidic bonds. It is obtained by the deacetylation of chitin (Fig. 3d). Notably, the physicochemical properties of chitosan are influenced by the degree of deacetylation. When the deacetylation level exceeds 55 %, chitosan can dissolve in dilute acidic solutions [101–103]. Chitosan is capable of undergoing cross-linking, esterification, and etherification reactions, primarily due to the presence of functional groups such as hydroxyl and amino groups. These functional groups are crucial for the reactivity of chitosan, which exhibits very high chemical and biological performance. Consequently, it has outstanding properties such as non-toxicity, good adsorption capacity, biocompatibility, and biodegradability.

2.2. Conversion of low molecular weight substances into high molecular weight polymers

From the perspective of biomass polymeric materials, these polymers primarily originate from natural resources such as plants, algae, and microorganisms. Their low molecular weight precursors include monosaccharides (such as glucose), amino acids, and fatty acids. Through polymerization reactions, these low molecular weight compounds form complex polymer structures, such as cellulose, starch, and polylactic acid, which exhibit excellent biocompatibility and biodegradability, as well as complex structures with high mechanical strength and thermal stability [104–108]. These characteristics render them promising for a variety of industrial applications, particularly in the fields of packaging materials and biocomposite materials. In addition, these synthetic polymeric materials have attracted attention due to their high specific surface area and good conductivity, which can effectively enhance the energy and power density of SCs. Therefore, the following sections will introduce the selection of low molecular weight compounds, the mechanisms of polymerization reactions, and the characteristics of polymeric materials, thereby providing a solid foundation for understanding the importance of biomass polymers in new materials and energy applications.

2.2.1. Selection of low molecular weight compounds

In the conversion process of low-molecular compounds, the selection of suitable low-molecular monomers is crucial for the success and performance of high-performance bio-based polymers. Various low molecular compounds, whether natural origin or synthetic monomers, provide a wide basis for polymer synthesis. Epoxides, as an important class of low molecular monomers, play a key role in polymerization reactions. Ethylene oxide is the most commonly used epoxide, which can be obtained through the epoxidation of plant oils and can also react with various additives under high-temperature conditions (Fig. 4a) [109]. Its unique molecular structure enables it to undergo ring-opening reactions during the polymerization process, resulting in the formation of polymers. In the ring-opening polymerization reaction, ethylene oxide reacts with active monomers under the influence of catalysts to produce polyethylene oxide, which can then be further processed to obtain the desired polymer forms, such as epoxy resins [110–114]. These epoxy resins, known for their superior mechanical properties and

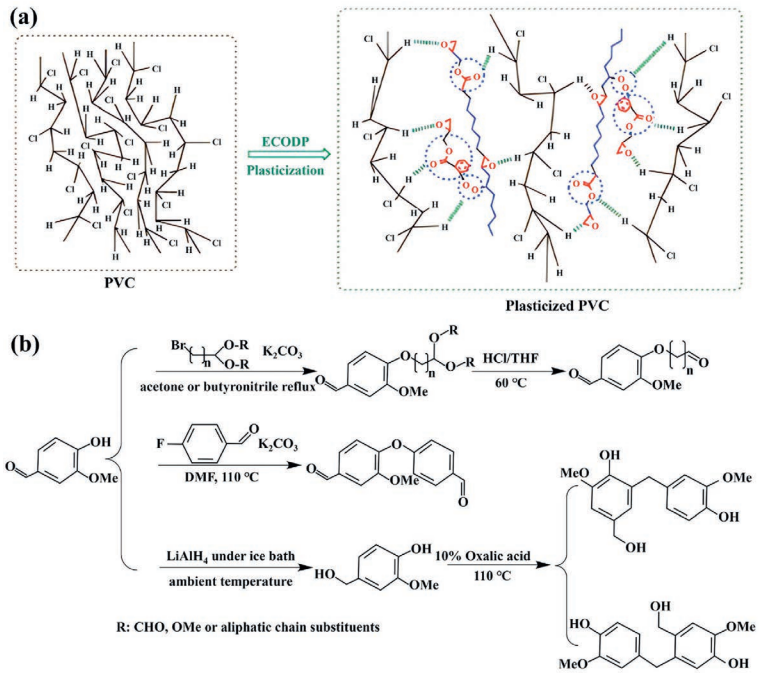


Fig. 4. Conversion from low molecular weight to high molecular weight polymer. (a) Chemical components of epoxidized vegetable oil. Reproduced with permission [109]. Copyright 2024, American Chemical Society. (b) Synthesis of phenolic resin. Reproduced with permission [131]. Copyright 2023, The Royal Society of Chemistry.

chemical stability, have been widely applied in the fields of coatings, adhesives, and composite materials.

Meanwhile, phenolic resins, as a classic cross-linked polymer, is synthesized based on the reaction between low molecular phenolic compounds and formaldehyde [115–117]. In this synthesis process, phenol and formaldehyde undergo a condensation reaction to form linear or cross-linked structures, ultimately resulting in phenolic resins that possess excellent heat resistance and mechanical strength. Phenolic resin has been widely used in electrical, construction and automobile industries due to its good electrical insulation and chemical corrosion resistance. The green synthesis of phenolic resins becomes possible by utilizing biomass-derived phenolic compounds, such as lignin or other natural polyphenols. Furthermore, the properties of the resin can be further optimized by adjusting the reaction conditions to meet the requirements of different applications.

Lactic acid, as a low molecular weight monomer, possesses excellent biocompatibility and biodegradability, and can be used to synthesize polylactic acid, which is extracted from starch or sugar through fermentation. The synthesis of polylactic acid requires the conversion of lactic acid monomers into high-molecular polymers through remodeling or polymerization reactions [118–121]. At the same time, appropriate temperature and catalyst are controlled in the reaction to obtain polymer properties suitable for specific applications. In addition, amino acids, as another important class of low molecular monomers, exhibit good biocompatibility and can form polyamide polymers through polymerization reactions. Amino acids not only exhibit good reactivity during polymer synthesis, but the properties of the final polymer can also be optimized by adjusting the use of different amino acids and the polymerization conditions. With the emphasis on environmental protection and renewable materials, the application of biomass-based low-molecular-weight monomers continue to expand. Low molecular monomers from different sources, such as sugars, amino acids and vegetable oils, have shown rich synthetic potential. By selecting suitable low molecular weight monomers, polymers with specific properties can be obtained.

2.2.2. Mechanism of polymerization reactions

The reaction of low molecular monomers under the action of catalysts or specific conditions to form high molecular polymers is a key process. Polymerization reactions can be roughly divided into two categories: chain polymerization and step polymerization [122–126]. Chain polymerization usually includes three stages: initiation, growth and termination, while step polymerization realizes polymer formation through the reaction between monomers. In the synthesis of polymers, specific catalysts play an important role in promoting reactions and enhancing polymerization efficiency. Meanwhile, reaction conditions such as temperature, pressure, and reaction time have significant effects on the molecular weight, molecular structure, and final properties of the polymers. The initiation phase of chain growth polymerization reactions is typically initiated by initiators that generate free radicals or cations, which then directly react with monomers to trigger the formation of the polymer chain. The propagation phase involves the continuous reaction of free radicals with other monomers, resulting in the formation of longer polymer chains. The termination phase can occur through chain transfer reactions or by converting the polymer chain into other forms to conclude the polymerization process. For instance, the synthesis of bio-based polyurethanes often involves the reaction between isocyanates and polyols, where isocyanates can be derived from the conversion of vegetable oils, resulting in polyurethane materials with diverse properties through the polymerization process. In contrast, in step polymerization, monomer molecules are directly connected to form polymers through chemical reactions such as dehydration condensation or addition reaction. This type of reaction usually does not require an initiator, and can be achieved simply by heating or adding a catalyst.

On the other hand, the crosslinking phenomenon of polymers plays a significant role in polymerization reactions. Crosslinking connects polymer chains through chemical or physical means to form a network structure, significantly improving the mechanical properties, thermal stability, and chemical resistance of the material [127–130]. For example, in the synthesis of phenolic resins, phenolic compounds react with formaldehyde under the influ-

ence of acidic or basic catalysts, producing a crosslinked three-dimensional network structure (Fig. 4b) [131]. The resulting resin exhibits excellent heat resistance and chemical stability. In addition, epoxy resins play an important role in modern materials and can be synthesized from natural monomers derived from plant resources. The crosslinking reactions of epoxy resins typically involve the reaction of epoxy groups with hardeners to form a network structure. In terms of thermal stability, mechanical properties, and environmental impact, epoxy resins synthesized from bio-based monomers exhibit excellent characteristics. Similarly, moderate adjustments to the distribution and structure of the epoxy groups can significantly enhance the properties of bio-based polymers.

During the polymerization process, the properties of the resulting polymer depend not only on the polymerization method and reaction conditions but are also closely related to the choice of monomers and their molecular structures. Furthermore, in the study of polymerization mechanisms, the observation of chain initiation and crosslinking reactions can provide an important theoretical basis for optimizing polymer design. In the synthesis of biomass-based polymers, the use of both physical and chemical crosslinking methods can enhance the tensile strength and toughness of the polymers.

2.2.3. Properties of macromolecular polymers

High polymer polymers, as an important category of materials, are widely applied in various fields, and their properties directly affect application performance. Common high polymer materials are derived from the conversion of low molecular compounds, particularly through polymerization using biomass resources, which has attracted increasing attention in recent years. Biomass-based high polymer materials can mitigate the environmental impact of traditional petroleum-based materials. Mechanical properties are important characteristics of high polymer materials, typically including strength, toughness, and ductility. For example, polylactic acid (PLA) is polymerized from lactic acid monomers, exhibiting good tensile strength and elastic modulus, which leads to its widespread application in fields such as medicine and packaging [132–134]. Research has shown that the thermal stability of PLA can be effectively enhanced through chemical crosslinking or copolymerization with other polymers. Moreover, these modified materials also possess good electrical conductivity, making them suitable for use as electrode materials in SCs. In the context of electrochemical energy storage devices, polymer electrodes not only require excellent mechanical strength to withstand repeated charge and discharge cycles but also need to have good electrical conductivity. Additionally, biomass-based polymers can have their mechanical properties optimized during the preparation process by controlling the degree of polymerization and crosslinking to meet the demands of high-performance energy storage devices. Biocompatibility is a significant advantage of bio-based polymers, especially in biomedical and environmental material applications. For instance, poly(3-hydroxybutyrate) (PHB) has gained considerable attention in drug delivery systems and tissue engineering due to its excellent biocompatibility and biodegradability [135–137]. Moreover, the degradability of polymers is a growing trend in the current development of materials science. Guided by the principles of sustainable development, the creation of biodegradable high polymer materials can not only reduce environmental pollution but also alleviate the burden on land through biodegradation. The preparation of biomass-based polymers not only enables the sustainable utilization of resources but also contributes to solving global environmental issues. Therefore, in the area of porous carbon electrode materials, the combination of the degradable characteristics, excellent mechanical properties, and thermal stability of biomass-derived polymer materials holds promise for further advancing the application of electrochemical energy storage devices such as SCs.

3. Preparation of biomass-based polymer-derived porous carbon

Carbon sources predominantly derive from plants, animals, and microorganisms. However, biomass polymers sourced from nature, as well as synthetic biomass polymers, cannot be utilized directly in the production of SCs. These polymers must undergo a complex carbonization and activation process to be transformed into activated carbon that is rich in porous structures, high in carbon content, and abundant in functional groups. The preparation of porous carbon derived from biomass-based polymers typically employs a classical two-step method. The first step is carbonization, which primarily aims to remove water and some small molecules of branched and side chains in biomass-based polymers to obtain biomass-based polymer molecules. The second step is activation, which usually utilizes physical or chemical activation methods to generate more pore structures, thereby increasing the specific surface area and pore volume. For porous carbon, a higher specific surface area signifies more active sites, thereby providing a larger contact area and enhancing electrochemical performance. At the same time, the size and distribution of the pore size directly affect the diffusion rate of the molecule in the material and its interaction with the pore wall. Raw materials and process conditions can significantly influence the yield, elemental composition, pyrolysis behavior, and specific surface area of biomass-based polymers, as shown in Table 1.

3.1. Pyrolysis and carbonization

Pyrolysis is one of the important methods for decomposing organic matter in biomass polymers (mainly cellulose, hemicellulose, and lignin) into unique forms of carbon materials, and it is also the most common and direct method. Biopolymers can be decomposed under anaerobic conditions at 300–1200 °C (Fig. 5a) [138,139]. Depending on the heating rate, pyrolysis can be classified into fast pyrolysis and slow pyrolysis. Fast pyrolysis is characterized by rapidly heating the feedstock, typically completed within seconds to minutes, with heating rates reaching hundreds to thousands of degrees per second. Fast pyrolysis can produce a large number of liquid products, with yields generally exceeding those of slow pyrolysis. The bio-oil generated has a high energy density, contributing to improved energy efficiency. Slow pyrolysis is usually conducted at temperatures between 300 °C and 700 °C and generally requires

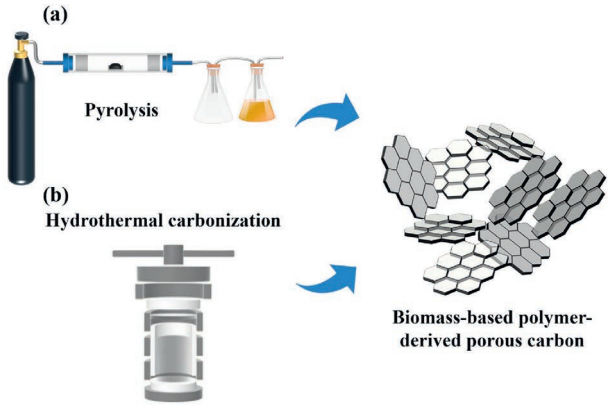


Fig. 5. The processes of pyrolysis and carbonization. (a) Schematic diagram of the pyrolysis process. Reproduced with permission [6]. Copyright 2024, Elsevier B.V. (b) Schematic diagram of hydrothermal carbonization. Reproduced with permission [8]. Copyright 2024, The Authors.

Table 1
Overview of factors affecting the properties of biomass-based polymers.

Factors	Yield	Element composition	Pyrolysis behavior	Specific surface area
Raw material type	Different raw materials can affect yield	Common elements include C, H, O, *etc.*	Different raw materials exhibit distinct pyrolysis behaviors	The specific surface area of different raw materials varies greatly
Temperature	High pyrolysis temperature may reduce yield, while low temperature may not achieve a high yield	Temperature changes may lead to an increase in the carbon (C) ratio	Higher temperatures tend to produce more gases and light oils, altering the distribution of pyrolysis products	Increased pyrolysis temperature generally leads to a higher specific surface area, especially during high-temperature pyrolysis
Atmosphere	An inert nitrogen atmosphere can enhance yield, while an oxidative atmosphere may decrease it	Changes in the oxygen content of the atmosphere may affect the elemental composition, leading to an increase in oxygen content	An oxidative atmosphere accelerates the pyrolysis reaction, altering pyrolysis behavior and gas products	The surface of products in an oxidative atmosphere may be more reactive, impacting specific surface area
Heating rate	Rapid heating typically enhances the yield	Rapid heating may lead to an uneven elemental composition	Heating rate affects the pyrolysis temperature profile	Quick heating promotes the formation of porous structures, often resulting in a larger specific surface area

several hours to even days for completion. It primarily generates biochar, resulting in lower amounts of liquid fuels and gases compared to fast pyrolysis, leading to a relatively lower overall energy utilization efficiency. Different characteristics and applications of products can be achieved depending on the biomass type and temperature used. At this stage of carbonization, the volatile components in the biomass polymer are removed, and water, volatile organic compounds, and gases (such as carbon dioxide and carbon monoxide) are released, leaving solid products rich in carbon. It is noteworthy that biomass undergoes decomposition and reorganization at high temperatures, leading to the breaking of the original polymer chains. This results in the formation of stronger carbon networks with C-C and C-H bonds, accompanied by the generation of higher-grade carbonaceous materials. The porosity and specific surface area of the resulting materials can be effectively controlled by adjusting the temperature, atmosphere, and carbonization time. The final porous materials not only exhibit a high specific surface area but also possess a favorable pore size distribution. The pore structure can take various forms, such as micropores (less than 2 nm), mesopores (2–50 nm), or macropores (greater than 50 nm), to meet different application requirements. The special hydrothermal carbonization is a technology that converts biomass-based polymers into carbonized products under hydrothermal conditions from 180 °C to 250 °C (Fig. 5b) [140–143]. Under certain temperature and pressure conditions, water molecules carry out hydrolysis and dehydration reactions on the biomass, breaking it down into small molecular substances. After several hours of reaction, these small molecular substances further react to form solid carbonaceous products, while also generating liquid bio-oil and gases. The hydrocarbons produced by hydrothermal carbonization contain a rich variety of oxygen-containing functional groups. These functional groups significantly facilitate the synthesis of porous carbon by increasing the number of reactive sites available for activation. Li *et al.* [144] used enzymatically hydrolyzed lignin as a carbon source to prepare three-dimensional hierarchical porous carbon. The resulting material exhibited a reasonable pore size distribution, with a specific surface area of up to 1504 m^2/g. porous carbon derived from biomass-based polymers has become an important direction in the research of new carbon materials due to its excellent performance, good tunability, and environmental friendliness. Furthermore, the functional groups on the surfaces of biomass-based polymer-derived porous carbon can be modified by changing the solvent medium during hydrothermal carbonization [145].

Microwave carbonization is a technology that serves as an alternative to traditional heating methods, particularly suited for biomass-based polymers with a high moisture content. Through microwave carbonization, the required temperature can be quickly reached in a short time, so as to obtain porous carbon materials of biomass-based polymers [146]. Zhou *et al.* [147] used mung bean shells as raw materials to compare two ultrafast methods for synthesizing boron-nitrogen co-doped porous carbon: hydrothermal carbonization and microwave carbonization. The results show that compared with hydrothermal carbonization, microwave carbonization can easily obtain a specific surface area of 813 m^2/g within 20 min. Flash carbonization is typically performed at a lower temperature of 400 °C, where biomass-based polymers are exposed to a gas flow for 5–10 min, allowing for rapid conversion into porous carbon. The carbon obtained through this method exhibits high yield and a higher micropore volume. Hirst *et al.* [148] successfully converted eucalyptus sawdust into carbon materials, with the flash carbonization method also retaining some of the "woody" morphology preserved from the sawdust. Torrefaction is a thermochemical conversion process, also known as mild pyrolysis, typically conducted at temperatures ranging from 200 °C to 300 °C for a duration of 10–60 min. The torrefaction process can occur under inert conditions or in a controlled oxidation environment. In such an environment, the calcination time and energy consumption can be reduced, and calcination helps to improve the combustion performance of biomass-based polymers. Zhong *et al.* [149] proposed a baking-mediated carbonization method, which demonstrated the ability to protect oxygen functional groups from escaping from porous carbon derived from reeds, effectively achieving oxygen doping and enhancing capacitance performance.

3.2. Physical activation

Physical activation utilizes water vapor, carbon dioxide, oxygen, air, or their mixed gases as activators to react with the atoms within carbon materials at high temperatures. This method is also known as gas activation [150–152]. Physical activation is divided into three steps: First, the carbon atoms and heteroatoms in the polymers, which have high reactivity, react with the activator to open the closed pores generated during the carbonization phase. In the second stage, the carbon atoms exposed in the previous phase react with the activator, expanding the original material's pore size in planes parallel and perpendicular to the carbon network, thereby creating a porous structure with a hierarchical pore size distribution, including macropores, mesopores, and micropores. The final stage involves competitive activation reactions, where the pore-expansion reactions dominate. Intense activation reactions lead to further expansion of the pores, potentially causing the pore walls to collapse and the walls of adjacent micropores to disappear, resulting in the formation of larger voids. Excessively high reaction temperatures and an abundance of activators can re-

sult in a more intense reaction, ultimately causing the biomass to carbonize into ash. The chemical reaction principles of physical activation can be explained by the following formula:

$$C + H_2O \rightarrow H_2 + CO \quad (1)$$

$$C + 2H_2O \rightarrow 2H_2 + CO_2 \quad (2)$$

$$CO + H_2O \rightarrow H_2 + CO_2 \quad (3)$$

$$C + CO_2 \rightarrow 2CO \quad (4)$$

$$2C + O_2 \rightarrow 2CO \quad (5)$$

$$C + O_2 \rightarrow CO_2 \quad (6)$$

It can be observed that these reactions are endothermic and need to be conducted at temperatures of 800–1000 °C. However, since expensive and corrosive chemical reagents are not used as activators, physical activation has a lower corrosivity to equipment, minimal environmental impact, and a relatively low production cost. Therefore, it is considered a simple and green method for the preparation of porous carbon materials.

The high-temperature physical activation process is conducive to the removal of disordered and poorly porous inorganic materials. Among the various physical activators, air and steam activation cannot be conducted at high temperatures. However, steam has a milder oxidation ability and is easier to control during the activation process. Porous carbon materials produced *via* steam activation have advantages such as uniform pore size, ease of operation, and environmental friendliness. First, water vapor molecules bind to the carbon surface, subsequently promoting the removal of single carbon atoms or small carbon clusters through an endothermic reaction, resulting in gas products. As carbon continues to be removed, the original carbon structure is gradually weakened, leading to the formation and expansion of pores. During the activation process, the resulting micropores and mesopores not only increase the specific surface area of the material but also improve its pore size distribution and adsorption properties. Furthermore, the temperature and concentration of water vapor have a significant impact on the activation effectiveness; appropriate reaction conditions can optimize the pore structure and enhance the performance of the final product. Noh *et al.* [153] prepared highly porous activated carbon using natural biomass polymer kenaf as the raw material through hydrothermal activation and steam activation methods. They further investigated the effect of steam flow time on the formation of active porous carbon. With the increase in steam flow time, the material exhibited an extremely porous and rough surface, leading to a more diversified combination of micropores and mesopores, and an increase in total pore volume, which is crucial for ion diffusion and ion adsorption in SCs. Additionally, under the conditions of 6 mol/L KOH, the assembled symmetrical SCs achieved an energy density of 4.86 Wh/kg at a power density of 2500 W/kg. Zhang *et al.* [154] used expired coffee as the raw material, contributing to waste reutilization and environmental protection (Fig. 6a). The expired coffee was first ground and then carbonized in a steam atmosphere. Due to physical activation, the derived carbon materials exhibited a lower surface area, high bulk density, and a rich presence of functional redox-active nitrogen and oxygen atoms (Fig. 6b). Moreover, these materials were able to achieve a specific capacitance of 312 F/g at a current density of 1 A/g. Zhang *et al.* [155] studied the preparation of porous activated carbon using potato mash as the raw material through steam activation. They constructed a symmetrical SCs

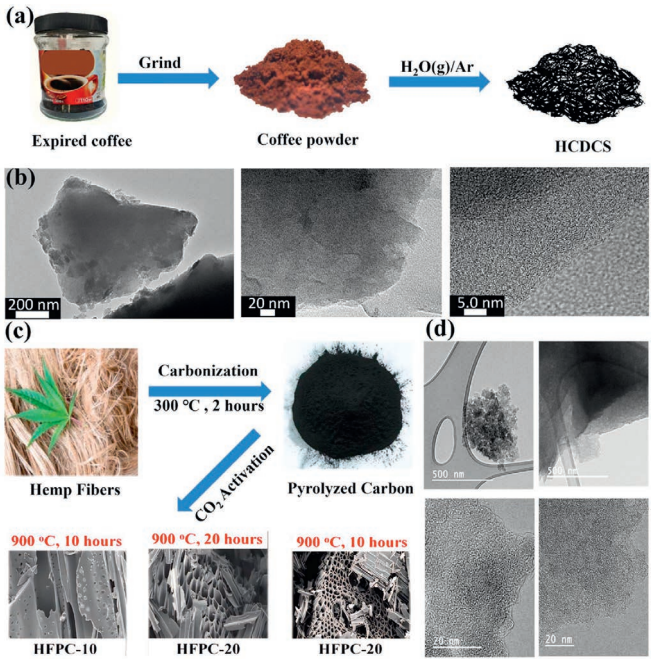


Fig. 6. Types of physical activation. (a) Schematic diagram of synthesis. (b) TEM images of derived porous carbon at different magnifications. Reproduced with permission [154]. Copyright 2022, Elsevier B.V. (c) Schematic diagram of porous carbon prepared from hemp fibers. Reproduced with permission [156]. Copyright 2021, Elsevier Ltd. (d) SEM and SAED images of Jamun seeds. Reproduced with permission [157]. Copyright 2023, Elsevier Ltd.

using the prepared potato-based activated carbon as electrode material. Building upon this, they investigated the impact of the mass loading of the electrode material and the influence of certain compressive stresses on the electrochemical performance of the SCs, thereby providing a feasible technique for enhancing energy storage in SCs.

In addition, among various physical activators, CO_2 is the mildest and most economical oxidizing gas. CO_2 activation facilitates the formation of pores in biomass-based polymers. Notably, the reaction rate between CO_2 and carbon materials is slower than that of steam and carbon materials, which leads to stricter reaction conditions. Relatively speaking, the slower etching rate makes CO_2 activation easier to operate and control. Gunasekaran *et al.* [156] used hemp fibers as raw materials, which were subjected to low-temperature carbonization followed by one-step synthesis of porous carbon through CO_2 physical activation (Fig. 6c). Since CO_2 is a chemically weak acid, the reaction rate is relatively slow, leading to a longer activation time. With extended activation time, the specific surface area and pore volume/size significantly increase. The carbon materials obtained through CO_2 activation exhibit a high specific surface area of 1060 m^2/g, thereby facilitating rapid ion transfer and efficient ion-electrolyte interactions. Rawat *et al.* [157] prepared biomass-based polymer-derived porous carbon using Syzygium cumini (Jamun) seeds, employing both acid treatment and CO_2 activation for the processing of the raw materials (Fig. 6d). The research results indicate that acid treatment can lead to partial structural collapse, while CO_2 activation results in a high specific surface area of 1000 m^2/g, with pore distribution across a wide range of micropores and mesopores. Further electrochemical analysis of the CO_2-activated carbon materials revealed good charge storage performance in symmetrics SCs, achieving a specific capacitance of 42.3 F/g at a current density of 0.1 A/g. In addition, Rawat *et al.* [158] also utilized lychee seeds as renewable raw materials. Lychee seeds are a major byproduct of the beverage and wine industries and are rich in starch. During the CO_2 physi-

cal activation process, CO_2 diffuses into the pores and is adsorbed onto the active sites of the biochar, resulting in partial gasification. Under conditions of 700 °C, symmetric capacitors made from the carbonized material achieved a specific capacitance of 190 F/g at a current density of 1 A/g. After CO_2 activation, the capacitance was significantly enhanced, reaching 493 F/g. Furthermore, during charge-discharge cycling in a 1 mol/L H_2SO_4 electrolyte, the capacitance retention rate remained above 90 %.

Compared to the chemical activation described below, research on the physical activation of biomass-based polymer-derived porous carbon is relatively scarce. Therefore, future studies should focus more on steam activation and CO_2 activation of biomass-based polymers, especially in the context of SCs applications. Physical activation techniques represent an important approach for achieving low-cost, green, sustainable, and large-scale industrial production of biomass-based polymer-derived porous carbon.

3.3. Chemical activation

Unlike physical activation, chemical activation occurs at lower temperatures (400–900 °C). Generally, after the raw materials are thoroughly mixed and come into contact with the activating agent, they undergo complex chemical reactions in a high-temperature environment, transforming into various derivatives. Subsequently, a significant number of pores are left behind through post-washing processes, resulting in the formation of highly porous carbon. During the activation process, many chemical reagents are used as activating agents. According to acid-base theory and activation mechanisms, activating agents can currently be classified into three types: acidic, basic, and neutral salts [159–163]. Different activating agents have varying effects on the structure and morphology of the products. In comparison, chemical activation has advantages such as low energy consumption, shorter activation times, higher yields, ease of control, and tunable porosity. Furthermore, the activation mechanisms of different activating agents may also vary; the following section will discuss this in detail. The comparison of different activators on the activation process and properties of porous carbon is shown in Table 2.

Acidic activating agents can effectively generate porous structures with various pore size distributions. During the activation process, both the quantity and acidity of the activating agent play a crucial role in determining the final pore structure. Acidic activating agents can rapidly diffuse into the material, leading to expansion and achieving uniform mixing of the activating agent and carbon precursor. This expansion effect allows for uniform heating of the acidic activating agent, providing high thermal stability while also reducing the activation temperature and time. Among all acidic activating agents, phosphoric acid (H_3PO_4) is the most commonly used. Its activation mechanism mainly includes five processes: Hydrolysis, dehydration, aromatization, cross-linking with biomass-based polymers, and pore formation. H_3PO_4 can effectively protonate the hydroxyl and ether

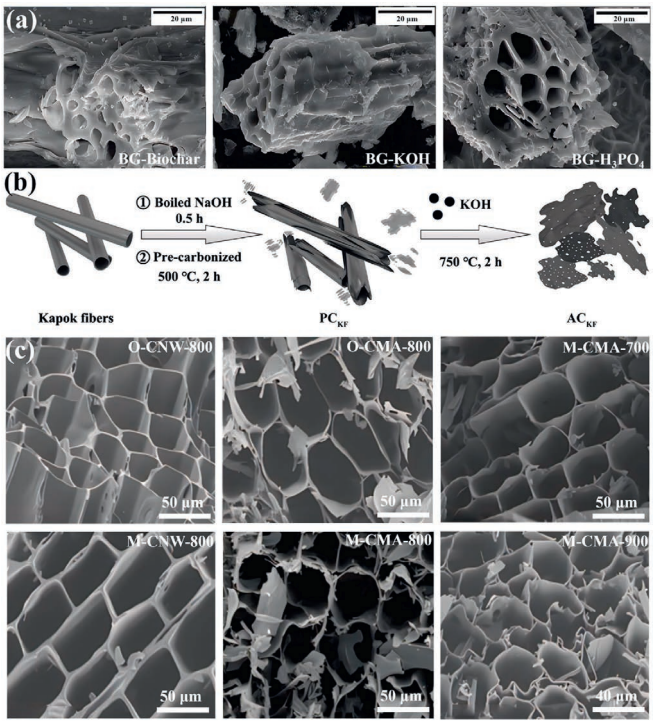


Fig. 7. Acid activation and alkaline activation. (a) SEM images of Bougainvillea leaves. Reproduced with permission [165]. Copyright 2024, Springer Nature. (b) Schematic diagram of the preparation of carbon derived from kapok fiber. Reproduced with permission [175]. Copyright 2024, Elsevier Ltd. (c) SEM images of natural larch waste wood carbonized under different conditions. Reproduced with permission [176]. Copyright 2024, Royal Society of Chemistry.

bonds in biomass, enhance its reactivity and promote structural reorganization by breaking and crosslinking through dehydration, decarboxylation and aromatization. Polysaccharides, proteins and degradation products rich in hydroxyl groups in biomass-based polymers are dehydrated, similar to the pyrolysis process. At high temperatures, H_3PO_4 facilitates the removal of alcohols or other oxygen-containing functional groups in the polymers and catalyzes the aromatization reaction, leading to the formation of highly stable aromatic ring structures. In the subsequent process, a large amount of H_3PO_4 and activated H_3PO_4 and biomass-based polymer composites were removed, leaving a large number of pores [164]. Gautam *et al.* [165] used bougainvillea flowers as raw material and employed two activating agents, H_3PO_4 and KOH, for the activation process (Fig. 7a). The results showed that both chemical agents were able to increase the surface area of the biomass-based polymers. Moreover, the micropore volume and surface area produced by H_3PO_4 activation were found to be higher than those obtained from KOH activation. The zinc-ion hybrid SCs assembled from the porous carbon materials derived from H_3PO_4 activation demonstrated efficient performance,

Table 2
Comparison of different activators on the activation process and characteristics of porous carbon.

Activators	Activation process	Characteristics of porous carbon	Ref.
KOH	Strong corrosivity High activation temperature is required	High specific surface area A large number of micropores and mesopores distribution	[162]
K_2CO_3	Low corrosivity High activation temperature is required	Medium-high specific surface area A large number of micropores and mesopores distribution	[143]
H_3PO_4	Strong corrosivity Lower activation temperature is needed	Wide specific surface area High phosphorus content A large number of micropores and mesopores distribution	[164]
$ZnCl_2$	Lower activation temperature is needed	Medium specific surface area Distribution of micropores and most mesopores	[163]

achieving a maximum energy density of 104.6 Wh/kg, which surpassed that of the zinc-ion hybrid SCs device assembled from KOH activation. The device also exhibited a coulombic efficiency of 86 % and a capacitance retention rate of 70 %. Jha *et al.* [166] reported the preparation of activated porous carbon with large specific surface area, wide micropore distribution and higher yield after carbonization from hemp stems by H_3PO_4 activation. Furthermore, they found that when this carbon material was assembled into symmetrical SCs devices, it achieved a significant cycling performance level of 98 % after 10,000 cycles at a current density of 1 A/g. Liu *et al.* [167] utilized sustainable ginkgo leaves as precursors to prepare porous carbon through a simple H_3PO_4 activation process. Notably, the H_3PO_4-activated ginkgo leaves exhibited a large number of interconnected pores, indicating that during the activation process, H_3PO_4 vibrated intensely in water to inhibit the aggregation of adjacent cell walls, and atoms were decomposed from polysaccharide molecules to connect *in situ*, forming layered pores. Subsequently, the polymer cellulose was hydrolyzed into oligosaccharides due to gas release, thereby creating the porous structure. Particularly, at a current density of 1 A/g, a high specific capacitance of 709 F/g was ultimately achieved. Peanut shells, as a valuable agricultural resource, are composed of lignocellulosic material rich in various abundant cellulose. Sandeep *et al.* [168] used peanut shells as the raw material, adding different activators and treating them at 200 °C for 7 h. Compared to other samples, the activated carbon treated with H_3PO_4 exhibited more defects due to the formation of phosphate groups and had a greater number of surface pores, which is beneficial for its electrochemical performance. In a three-electrode system, the energy density of the asymmetric SCs assembled from the H_3PO_4-activated porous carbon material was 4.08 Wh/kg, with a power density of 101.3 W/kg. Additionally, after 1200 charge-discharge cycles, the stability reached 90 %.

Numerous studies have shown that KOH is an effective and the most commonly used chemical activator, widely applied in laboratory-scale research. Biomass-based polymers can be converted into porous carbon with various morphologies and pore structures through KOH alkaline activation. The use of KOH as an activator can improve the reaction conversion rate while achieving a high specific surface area and porosity in the carbon material. Its oxidative action can produce oxygen-containing functional groups. The mechanism of KOH activation is based on the following reactions:

$$6KOH + 2C \rightarrow 2K + 2K_2CO_3 + 3H_2 \quad (7)$$

$$K_2CO_3 \rightarrow K_2O + CO_2 \quad (8)$$

$$K_2CO_3 + 2C \rightarrow 2K + 3CO \quad (9)$$

$$K_2O + C \rightarrow 2K + CO \quad (10)$$

$$CO_2 + C \rightarrow 2CO \quad (11)$$

During the activation process, the carbon material first reacts with KOH, generating K_2CO_3 and H_2 at the active sites. Subsequently, K_2CO_3 further decomposes to produce CO_2 and H_2O. The generated H_2O and CO_2 can promote the development of pore volume through physical activation reactions. When the temperature exceeds 600 °C, the reaction with KOH is complete, while K_2CO_3 begins to decompose above 700 °C and disappears from the system at 800 °C. Meanwhile, the produced potassium vapor interacts with the carbon material. Lastly, residual alkaline substances and metal salts can be removed through acid washing and rinsing, an operation that also generates new pores. Different biomass-based polymers can be utilized to prepare porous carbon materials with varying morphologies, pore structures, and surface functional groups, further influencing their applications in energy storage [169–174]. Zheng *et al.* [175] utilized cotton fibers as raw materials to prepare two-dimensional bio-nanosheets through a simple KOH activation process. Due to the activation of KOH, the specific area of the raw material increased sharply (Fig. 7b). It is speculated that the activation has a great damage to the wall of the kapok fiber, resulting in the influence of the layered structure. In 6 mol/L KOH electrolyte, the carbon material exhibits a high specific capacitance of 405 F/g at a current density of 1 A/g. In addition, the material also has good rate performance and cycle stability. Luo *et al.* [176] utilized waste wood from larch as the raw material to prepare self-supporting carbon electrodes with a layered structure through a specialized carbonization and activation process (Fig. 7c). These samples possess a stable self-supporting microtube array structure, with a specific surface area reaching 945.09 m^2/g, indicating that porosity was further enhanced after KOH activation. In comparison with other samples, the optimized samples exhibited excellent specific capacitance, achieving 211.3 F/g at a current density of 0.5 A/g, and maintained 98 % of their capacitance even after 8000 cycles. Li *et al.* [177] developed a simple and effective carbonization activation process to prepare porous carbon materials derived from rice husks. During the alkali activation process, the samples carbonized at 900 °C exhibited a coral reef-like structure surrounded by scales, which can be attributed to the effects of alkali etching. This activation etching exposes more active sites, provides a larger contact area for ion transport, and thus enhances the electrochemical performance, improving the applicability of biomass-based polymers in the field of SCs. Liang *et al.* [178] employed a soul-gel method to prepare three-dimensional carbon materials derived from phenolic resin and ammonium alginate. The phenolic alginate composite porous carbon exhibits a coral network structure of particle clusters under low magnification. As the alkali-to-carbon ratio increases, the carbon framework experiences more severe etching, leading to an increase in pore size and the development of a more extensive porous network, which facilitates rapid ion transport. Additionally, the size of each particle within these clusters' ranges from tens to hundreds of nanometers, providing a greater specific surface area. This three-dimensional coral-like interconnected structure of carbon materials, when used as electrodes, can further enhance the activation efficiency of SCs. Tian *et al.* [17] employed a green and simple method to synthesize a resorcinol-furfural resin using resorcinol and biomass furfural as raw materials, and directly prepared three-dimensional layered porous carbon materials through a one-step carbonization and activation strategy. During the cross-linking process of the resin, a significant amount of KOH particles was captured *in situ*, and as the amount of KOH increased, more channels gradually emerged. The material achieved a specific capacitance of 291 F/g at a current density of 0.1 A/g. Notably, the assembled symmetric device demonstrated an energy density of up to 18.5 Wh/kg.

In addition to KOH activation, $ZnCl_2$ also plays a positive role in the formation of pores. During the heat treatment process, $ZnCl_2$ does not react directly with carbon, but it promotes the dehydration and aromatic condensation of biomass-based polymers. In the activation process, $ZnCl_2$ acts as a dehydrating agent, removing oxygen in the form of water and demonstrating a deoxygenation effect under high-temperature conditions, thereby facilitating the formation of porous carbon. First, at 600 °C, $ZnCl_2$ is converted into hydrated $ZnCl_2$, thereby achieving dehydration. Following this, the hydrated $ZnCl_2$ formed in the first step further decomposes into ZnOCl; finally, ZnOCl degrades into ZnO and CO_2. The following equations detail this process:

$$2ZnCl_2 + O_2 \rightarrow 2ZnCl + Cl_2 \quad (12)$$

$$2ZnO + C \rightarrow 2Zn + CO_2 \quad (13)$$

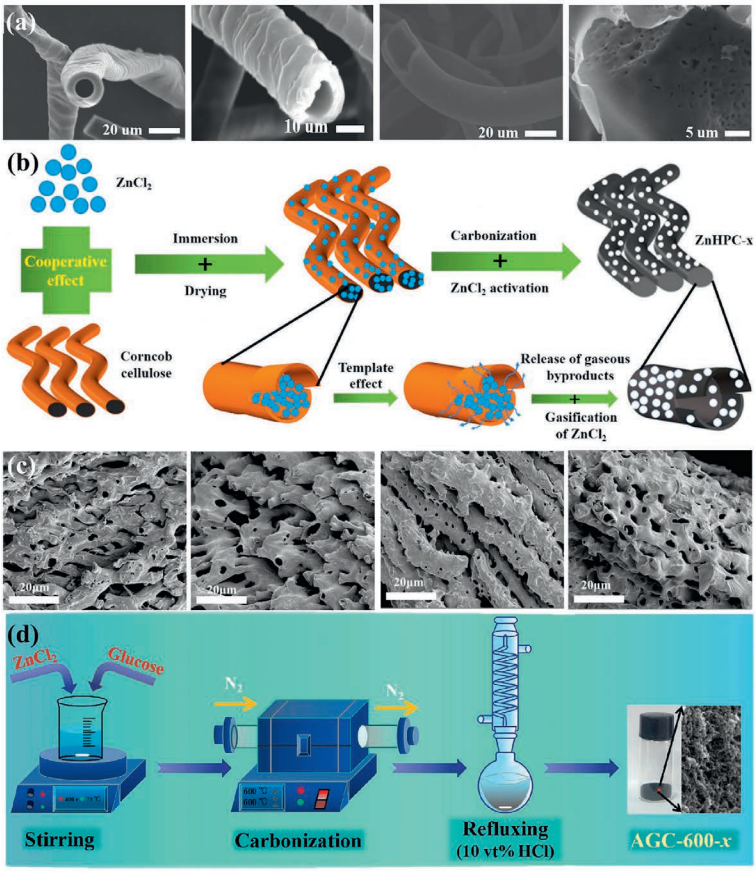


Fig. 8. Salt activation. (a) SEM images of samples prepared under different conditions. Reproduced with permission [179]. Copyright 2021, Elsevier B.V. (b) Activation process of corn cob fibers and $ZnCl_2$. (c) SEM images of samples after activation of corn cob fibers and $ZnCl_2$. Reproduced with permission [180]. Copyright 2022, Elsevier B.V. (d) Schematic diagram of the preparation of porous carbon. Reproduced with permission [181]. Copyright 2020, Elsevier B.V.

Although the microporous carbon produced by KOH activation has a very high specific surface area, not all micropores are effectively utilized, which limits ion transport and leads to suboptimal performance in energy storage applications. In contrast, the porous carbon activated by $ZnCl_2$ exhibits both micropores and small mesopores, providing more surface sites and channels for the formation of electric double layers and ion diffusion. Tang *et al.* [179] proposed a method for preparing activated carbon from waste sheep wool through chemical activation and carbonization (Fig. 8a). Notably, the activated carbon that is activated using a 30 % $ZnCl_2$ solution and carbonized in air at 500 °C exhibits the highest specific surface area, reaching up to 533.17 m^2/g. Erman Taer *et al.* used banana stem fibers as raw materials to prepare porous carbon, selecting a 0.5 mol/L $ZnCl_2$ solution as the activating agent. The study demonstrated that $ZnCl_2$ as an activating agent could separate the banana stem fibers and reduce the fiber diameter. Moreover, the carbon electrodes made from banana stem fibers exhibited excellent performance in SCs, with a specific capacitance of 179 F/g, a power density of 6.19 Wh/kg, and an energy density of 44.67 W/kg. Yang *et al.* [180] used corn cob cellulose as the raw material to prepare hierarchical porous carbon through a one-step activation process for the carbon cathode of zinc-ion mixed capacitors (Fig. 8b). $ZnCl_2$ acts as an activator to adjust the porosity, and its solution can penetrate into the natural pore channels of cellulose. At the same time, $ZnCl_2$ acts as a template in an *in-situ* occupying manner to prevent the agglomeration of adjacent cell walls, thereby forming a rich porous structure and high specific surface area. Such a well-developed porous structure ensures the easy transport of Zn^{2+} ions and high-capacity storage (Fig. 8c). Furthermore, the optimized hierarchical porous carbon-based zinc-ion mixed capacitors exhibited a high specific capacity of up to 120.3 mAh/g, maintaining 99.2 % long-cycle stability after 10,000 cycles at a current density of 5 A/g. Feng *et al.* [181] used $ZnCl_2$ as the activating agent to prepare porous activated carbon materials derived from glucose (Fig. 8d). $ZnCl_2$ exhibits catalytic dehydration and template effects, resulting in a highly heterogeneous surface of the raw materials. Meanwhile, the release of gases such as H_2O, CO_2, and others promotes the formation of pores, which is beneficial for increasing the surface area and enhancing the wettability of the electrolyte. In a three-electrode system, the specific capacitance reached 176.75 F/g at a current density of 1 A/g. Additionally, the assembled symmetric SCs demonstrated an energy density of 17.99 Wh/kg at a power density of 399.94 W/kg, with only an 8.1 % loss in capacitance after 10,000 charge-discharge cycles.

In summary, during the chemical activation process, the addition of activating agents induces the formation of micropores within the raw materials. Among various chemical reactions, KOH, $ZnCl_2$, and H_3PO_4 are the three most widely studied activating agents. Due to the large amounts of these activating agents, along with high activation temperatures and prolonged activation times, the micropores may transform into mesopores or macropores after etching. However, intense activation conditions may also lead to the burning through and melting of the pore walls. Therefore, by effectively controlling the activation conditions, it is possible to fabricate three-dimensional layered porous carbon with well-developed porosity. In addition, combining both physical and chemical activation can open up broader possibilities for altering

Table 3
Comparative analysis of biomass-based polymers for deriving porous carbon and supercapacitors performance.

Biomass-based polymer	Structural characteristics	Methods for deriving porous carbon	Advantages	Disadvantages	Supercapacitor performance	Ref.
Cellulose	Linear, high crystallinity	Carbonization-activation	Widely available, low cost, good biocompatibility	High carbonization temperature required, poor tensile strength post-carbonization	High specific capacitance (276 F/g)	[169]
Proteins	Protein chains, folded structure	Enzymatic hydrolysis-carbonization-post-treatment	Rich amino acid structure, easy to modify	Difficult purification, performance affected by fat impurities	High specific capacitance (270 F/g)	[170]
Sodium alginate	Helical structure	Carbonization-activation	Good biodegradability, environmentally friendly	Poor stability, low mechanical strength	Higher specific capacitance (322 F/g)	[171]
Starch	Polysaccharide structure, nonlinear	Carbonization-activation	Abundant source	Structure prone to changes, poor stability	High specific capacitance (172 F/g)	[172]
Carboxymethyl Cellulose-Bacterial Cellulose Composite	Composite structure, flexible	Carbonization-physical/chemical activation	Excellent overall performance	Complex processing of composite materials	Higher specific capacitance (350 F/g at 0.5 A/g)	[173]
Gelatin	Protein polymer, flexible structure	Carbonization-activation	Low cost, readily available	Poor structural stability	Superior specific capacitance (392 F/g)	[174]

the properties of the materials. Table 3 compares the structural characteristics of biomass-based polymers, the preparation methods of derived porous carbon along with their advantages and disadvantages, and the performance of SCs.

4. Novel modifications of biomass-based polymer-derived porous carbon to enhance supercapacitors performance

High specific surface area porous carbon materials can be achieved through pyrolysis, carbonization, physical activation, and chemical activation. However, traditional physical activation synthesis strategies have drawbacks such as high energy consumption, long processing times, and difficulties in control. Although chemical activation can provide good activation effects at relatively low temperatures, it also faces issues such as severe reactor corrosion, the cost and safety of chemical reagents, and difficulties in post-treatment. In recent years, researchers have continuously explored novel and efficient strategies to further enhance the performance of SCs. These innovative strategies can generally be classified into three main categories: Doping techniques, copolymerization methods, and the design and preparation of nanocomposites.

4.1. Heteroatom doping

Currently, in the context of research on biomass-based polymer-derived porous carbon materials, only limited activation methods may not achieve the desired levels of electrochemical performance. To enhance the properties of carbon materials, the incorporation of heteroatoms into the carbon matrix can be considered. This process can significantly alter various characteristics of the material, including the introduction of functional groups, improvements in electronic conductivity, wettability towards electrolytes, and the adjustment of interlayer spacing. Common heteroatoms such as nitrogen, oxygen, sulfur, and phosphorus can effectively introduce defect structures by altering the carbon framework and disrupting Π-Π symmetric conjugation, thereby significantly enhancing the surface characteristics of the materials [182–187]. These modifications not only meet the specific application requirements of SCs but also provide new ideas and directions for the development of novel high-performance energy storage materials.

Nitrogen is commonly used for heteroatom doping in carbon materials, and the incorporation of nitrogen into the carbon matrix does not alter their fundamental structure. Furthermore, nitrogen-carbon functional groups exhibit greater electrochemical stability compared to carbon-oxygen functional groups. This is because the N atom has one more electron in the valence electron layer than the carbon atom, which can act as an electron donor, resulting in an increase in the number of free electrons in the material. Additionally, the electronegativity of N is higher than that of C, which further promotes the adsorption of electrolyte ions and enhances hydrophilicity, facilitating sufficient contact between carbon electrodes and the electrolyte. Nitrogen doping in carbon materials can exist in various chemical forms, primarily including pyridine-N, pyrrole-N, quaternary-N, and pyridine-N oxide. Among these, pyrrole nitrogen and pyridine nitrogen are particularly important for enhancing pseudocapacitance. Another advantage of N doping is that it can prevent the formation of hydrocarbons in the lattice. It is known that hydrocarbons reduce the performance of SCs by generating a dielectric dead layer. At the same time, the content of N has an important influence on its electrochemical performance. Therefore, optimizing the nitrogen content is also crucial for achieving optimal performance from the electrodes. Li *et al.* [188] prepared N-doped hierarchical porous carbon nanosheets using sodium alginate containing Zn-2-methylimidazole complex as raw material. Sodium alginate, as a natural biomass-based polymer, has attracted much attention due to its wide range of sources and environmental friendliness. Although the introduction of coordinating polymers did not alter the sheet morphology, it facilitated the formation of macropores. This is likely due to the large number of volatile substances generated during the decomposition of the coordinating polymers, which created numerous macroporous structures upon their escape. Due to the layered structure and N doping, the resulting carbon material exhibited excellent electrochemical performance as an electrode material for SCs, demonstrating a specific capacitance of 210.4 F/g at a current density of 2 A/g. Kim *et al.* [189] used protein-rich mealworm as a raw material for the preparation of porous carbon materials, mainly through the synergistic action of amino acids and fatty acids within the mealworm (Fig. 9a). Nitrogen doping can provide defects inside the carbon structure, thereby enhancing the active sites of energy storage and improving the conductivity of carbon materials, thereby improving the specific capacity and energy storage efficiency. The mealworm-based nitrogen-doped porous carbon electrodes exhibited excellent specific capacitance at both low and high current densities. At a current density of 0.2 A/g, the specific capacitance was 154.8 F/g, while at a current density of 5 A/g, it was 137 F/g, primarily attributed to the nitrogen-doped carbon structure generated during the activation process (Fig. 9b). Tian *et al.* [190] successfully prepared resorcinol/urea-furfural resin by using clean and environmentally friendly furfural as raw material

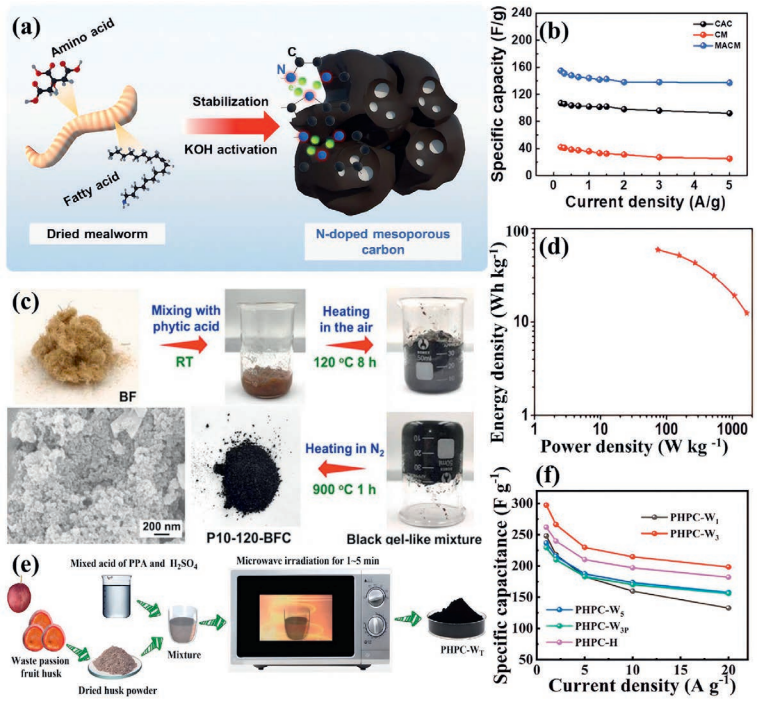


Fig. 9. N and P doping. (a) The process of preparing porous carbon using mealworms as the substrate. (b) Specific capacity at a current density of 0.2–5 A/g. Reproduced with permission [189]. Copyright 2024, Springer Nature. (c) Preparation process of bamboo fiber-doped phosphorus-derived carbon materials. (d) Energy densities. Reproduced with permission [191]. Copyright 2024, Elsevier B.V. (e) Proposal for the preparation of phosphorus-doped layered porous carbon using microwave irradiation method. (f) Specific capacitance of the prepared samples at different current densities. Reproduced with permission [193]. Copyright 2022, Elsevier Ltd.

and co-crosslinking with resorcinol and urea under the action of catalyst, in which urea was used as the source of nitrogen doping. A unique ant nest-like three-dimensional interconnected structure was formed during the preparation process. Notably, this porous carbon material exhibited a specific capacitance of 283 F/g, and the assembled symmetric devices maintained a capacitance retention rate of 92 % after 50,000 cycles, demonstrating excellent cycling stability. He *et al.* used pomelo peel as raw material to prepare N-doped derived porous carbon by a combination of hydrogel dispersion activation and freeze-drying. As a good precursor of carbon materials, pomelo peel is rich in plant fibers, a large number of functional groups (hydroxyl, carboxyl, amino) and highly porous structure. Additionally, the presence of pyrrole-N and pyridine-N in the carbon material can provide electron lone pairs to the conjugated carbon system, enhancing the surface activity and wettability for electron transfer reactions. The layered carbon materials exhibit a suitable pore structure, level of heteroatom doping, and high specific surface area, demonstrating excellent specific capacitance, reaching 438 F/g at a current density of 0.5 A/g. Notably, at a power density of 174.9 W/kg, a high energy density of 59.5 Wh/kg was achieved.

The incorporation of phosphorus into carbon matrices as a technique to improve the electrochemical performance of carbon-based materials has been widely studied. Since phosphorus and nitrogen belong to the same group in the periodic table, they exhibit similar chemical properties in carbon materials. Specifically, phosphorus is embedded in the carbon skeleton through the P-C bond, and the interaction between the phosphorus atom and the surrounding carbon atom enables it to redistribute the charge density of the carbon layer. Moreover, phosphorus-doped carbon materials, due to their larger atomic radius and electron-donating capability, can increase the defect sites and interlayer spacing in carbon crystals, thereby generating more active sites and defects. This promotes electron transfer and electrolyte ion diffusion, significantly enhancing the electrochemical performance. Zheng *et al.* [191] prepared phosphorus-doped porous carbon using bamboo fiber and phytic acid. It is worth noting that the higher pretreatment temperature and the appropriate amount of phytic acid in the pretreatment process contribute to the formation of porous carbon with rich pore structure (Fig. 9c). The resulting phosphorus-doped porous carbon exhibits a specific surface area of up to 1229 m^2/g. The zinc-ion hybrid SCs made from this carbon achieves a specific capacity of 109 mAh/g in a 2 mol/L $ZnSO_4$ electrolyte. Furthermore, phosphorus doping significantly enhances the energy density, with the maximum energy density of the flexible solid-state zinc-ion SCs assembled from the prepared carbon material reaching 60 Wh/kg and the maximum power density reaching 1653 W/kg (Fig. 9d). Guo *et al.* [192] carbonized phenolic resin and subsequently activated it with KOH to prepare phosphorus-doped layered porous carbon aerogels. The incorporation of phosphorus in the carbon matrix leads to asymmetric charge density, enhances asymmetric spin density, and increases the charge delocalization of carbon atoms. Consequently, the phosphorus-doped carbon exhibits a hierarchical porous structure. After activation at 800 °C, the material exhibits a good capacitance of 406.2 F/g in 6 mol/L KOH. When the power density is 200 W/kg, the energy density of the prepared sample is as high as 16.97 Wh/kg. In addition, after 100,000 charge-discharge cycles, the specific capacitance of the prepared sample did not decay. Meng *et al.* [193] developed a super simple microwave irradiation method to prepare phosphorus-doped layered porous carbon using discarded passion fruit shells as raw materials (Fig. 9e). The resulting material has a specific surface area of up to 1858.2 m^2/g, exhibiting good conductivity and enhanced wettability. The prepared phosphorus-doped layered porous carbon can be stably charged and discharged in a trifluoroacetic acid electrolyte in a wide voltage window of 1–0.5 V under a three-electrode structure, and has a high specific capacitance of up to 297.1 F/g at a current density of 1 A/g (Fig. 9f). Additionally, the symmetric SCs devices assembled using this material and tri-

fluoroacetic acid electrolyte can operate stably at 1.5 V, maintaining a high capacitance retention rate of 94.9 % after 30,000 cycles.

Sulfur is also a heteroatom that can be doped into carbon materials, but there are relatively few studies on N, P and other elements. The atomic radius of sulfur is larger than that of nitrogen and phosphorus, which results in a greater interlayer spacing in sulfur-containing compounds under activation, thus allowing them to maintain a stable structure during the insertion and separation of electrolyte ions. Moreover, the incorporation of sulfur atoms can lead to the deformation of carbon materials, creating more vacancies and defects, which promotes the exposure of active sites and may significantly enhance the interfacial contact between the active sites and the electrolyte. Singh *et al.* [194] prepared highly porous sulfur-doped activated carbon using bagasse as the raw material. The fibrous stems of sugarcane contain lignocellulosic materials composed of cellulose, hemicellulose, lignin, and various inorganic elements, which are often used as precursors for carbon materials. The introduction of sulfur powder in the experiment is beneficial to the formation of sufficient S^{2-} ions by thermal decomposition. Furthermore, the sulfur-doped porous carbon materials derived from waste sugarcane bagasse possess a large amount of mesopores, which shortens the ion diffusion path and enhances the ion transfer efficiency. The experimental results show that the material has a high specific capacitance of 282.25 F/g at a circuit density of 0.1 A/g, and maintains 96.6 % capacitance after 10,000 cycles, showing good cycle stability. Huang *et al.* [195] prepared nitrogen and sulfur co-doped hierarchical porous biomass-based polymeric carbon using mantis shrimp shells as the carbon precursor. The shrimp shell is composed of crystalline nanofibers and mineral nanoparticles composed of abundant chitin (β-(1,4)—2-acetamido-2-deoxy-D-glucopyranose). Moreover, the pyrolysis of nitrogen and sulfur-doped biomass-based porous carbon is beneficial for improving specific capacitance, as the heteroatoms enhance surface wettability and provide additional pseudocapacitance. The results show that the prepared carbon material has a uniform dendritic structure, and nitrogen and sulfur atoms are successfully introduced into the carbon skeleton. At an activation temperature of 750 °C, the specific surface area can reach up to 401 m^2/g, and with high nitrogen and sulfur content, the specific capacitance of the material can achieve a maximum of 201 F/g. Yin *et al.* [196] successfully prepared a porous N/S dual-doped carbon material using renewable biomass lignin as raw material (Fig. 10a). At the optimal temperature of 700 °C, the specific capacitance of the synthesized doped carbon material reached a maximum of 240.6 F/g. At the same time, the material also showed good electrochemical stability. At a current density of 10 A/g, the specific capacity remained 95.0 % after 3000 charge-discharge cycles (Fig. 10b).

Other heteroatoms, such as oxygen and boron, also contribute to the electrochemical performance of carbon materials. Adding O to carbon materials will produce functional groups that bind to the surface, such as -COOH and C-O, which can promote the surface wettability of biomass-based polymer-derived carbon. By controlling the amount of doped oxygen atoms, more hole states can be introduced, thereby improving the performance of SCs. Zhong *et al.* [149] employed a carbonization strategy mediated by roasting to prepare oxygen-doped porous carbon derived from reed (Fig. 10c). The prepared carbon material has a specific surface area of 1650 m^2/g and contains abundant 9.63 % oxygen-containing functional groups, which can promote ion transport and improve capacitance performance. The roasting pretreatment mainly reduces the loss of oxygen elements during the preparation process. Oxygen doping provides additional pseudocapacitance, resulting in an exceptionally high capacitance of up to 336.4 F/g, with a high-rate performance of 76.1 % achievable at current densities ranging from 1 A/g to 10 A/g (Fig. 10d). Boron, as a dopant for carbon-based materials, also exhibits substantial potential. This is because the boron atom has one valence electron less than the carbon atom, showing a lack of valence electrons. Introducing boron atoms into the carbon lattice produces a p-type doping effect, as boron atoms accept electrons from adjacent carbon atoms, thereby creating a vacancy within the lattice. In SCs, boron doping can attract electrons in a negatively charged electrolyte to enhance the capacitance of the electrode. Du *et al.* [197] prepared hierarchically porous boron-doped carbon materials using glucose as the raw material through a simple activation and doping strategy (Fig. 10e). The B-doped process can improve the wettability of the carbon electrode surface, thereby enhancing the effective penetration of electrolyte ions and their interaction with the carbon electrode surface. The results indicate that the boron-doped carbon material exhibits a high specific capacitance of 379.9 F/g at a current density of 1 A/g (Fig. 10f), and the SCs maintains a capacitance retention rate of 96.3 % after 10,000 cycles, demonstrating excellent cycling performance. Wang *et al.* prepared boron and sulfur co-doped porous carbon materials using boric acid and thiourea as the sources of B and S, respectively, employing a $ZnCl_2$ activation method. The resulting electrodes are rich in heteroatoms, with a B content reaching 5.56 %, achieving a specific capacitance of 290.7 F/g at a current density of 0.5 A/g. In addition, a specific energy of 16.65 Wh/kg can be achieved at 450 W/kg when assembling a symmetrical SCs.

By introducing heteroatoms (such as N, P, S, O, B) into carbon materials, it is possible to significantly enhance the performance of carbon-based electrodes. In recent years, many researchers have not only focused on a single element, but also studied the co-doping of multiple elements. Numerous published papers have demonstrated that co-doping (N/O, N/P, N/S, N/S/P, *etc.*) has considerable potential in SCs electrode materials. Zhou *et al.* [198] employed a simple molecular self-assembly method to synthesize lignin-based carbon nanotubes, and achieved co-doping of nitrogen and sulfur during the subsequent carbonization and activation process. Ultimately, a specific capacitance of 391.4 F/g was obtained at a current density of 0.5 A/g. Li *et al.* [199] used orange peels as the raw material and employed boric acid and diammonium phosphate as co-dopants to prepare B/N/P co-doped porous carbon. The results showed that the material exhibited a superior specific capacitance of 289 F/g at 5 A/g, and after 10,000 cycles, the capacitance retention rate reached 93.6 %. Compared with single doping, the synergistic effect of multiple heteroatoms in co-doping can provide more active sites, thereby improving the electrochemical performance of carbon-based materials and promoting the realization of high electroactive density.

In summary, the doping of foreign atoms (such as N, P, S, O, and B) is widely recognized for its ability to improve the conductivity, wettability, and additional capacitance of materials by adjusting the surface properties of the electrodes. In addition, co-doping may also lead to the redistribution of charge, resulting in a synergistic effect, thereby further improving the overall performance of the electrode. The next copolymerization part will further explore the formation strategy of composite materials that optimize conductivity and energy storage characteristics.

4.2. Copolymerization

Biomass-based polymer and conductive polymer composites are considered one of the most promising choices for SCs materials. Conductive polymers include polyaniline, polypyrrole, polythiophene, and poly(3,4-ethylenedioxythiophene), among others [200–203]. Conducting polymers exhibit pseudocapacitance characteristics due to their redox reactions, which are conducive to the storage and release of charges. Among them, the conjugated Π bond on the polymer chain can achieve conductivity through a reversible redox reaction, thereby providing a higher specific ca-

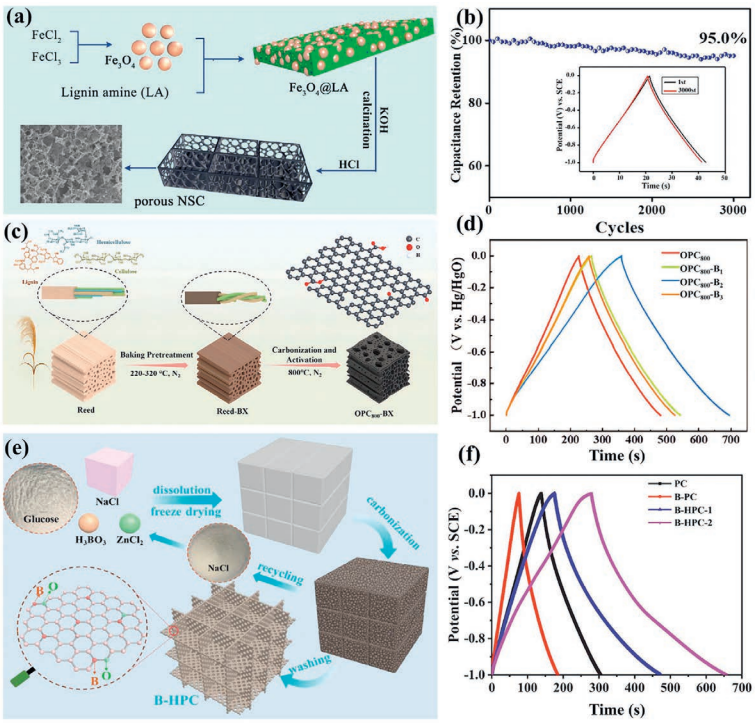


Fig. 10. Sulfur doping and doping with other atoms. (a) Synthesis route of porous N/S-doped materials. (b) Stability at 10 A/g. Reproduced with permission [196]. Copyright 2020, Elsevier B.V. (c) Schematic diagram for the preparation of O-doped porous carbon. (d) GCD curves at 1 A/g. Reproduced with permission [149]. Copyright 2023, Elsevier B.V. (e) Schematic diagram of the preparation process for B-doped porous carbon. (f) Comparison of GCD curves at a current density of 1 A/g. Reproduced with permission [197]. Copyright 2021, Elsevier Ltd.

pacitance. However, the insertion and detachment process caused by the cyclic charge and discharge of ions may lead to the rupture and shedding of conductive polymers. In order to fully harness the potential of these polymers, the combination of carbon materials with conductive polymers has become a focal point in this research field. When conductive polymers polymerize within the pores of porous carbon, they interact with the surface of the carbon materials through physical adsorption and chemical bonding, which helps to enhance the bonding strength of the composites. Additionally, conductive polymers possess a certain level of conductivity, and their distribution and arrangement within the porous carbon will influence the overall electrical conductivity properties. At the same time, the electrical conductivity of conductive polymers enhances the coupling of electrons, thereby improving the efficiency of the energy storage or energy release processes. Gao *et al.* [204] used lotus leaves as raw materials due to the high content of lignocellulose in both the leaves and petioles, which is conducive to the preparation of high-yield carbon materials (Fig. 11a). They prepared carbon derived from lotus leaves and carbon derived from lotus petioles through carbonization and KOH activation; but the low energy density limits further development. In order to improve this problem, they used polyaniline to modify the derived carbon materials and prepared composite materials by *in-situ* polymerization. The introduction of polyaniline provided Faradaic capacitance, and the synergistic effect between the derived carbon materials and polyaniline resulted in a high specific capacitance of 1332.5 F/g at a current density of 0.3 A/g for the synthesized composites. Furthermore, a symmetrical SCs device assembled from two electrodes exhibited an energy density of 75.7 Wh/kg at a power density of 540 W/kg (Fig. 11b). Fu *et al.* [205] employed three different geometries of lignin-derived porous carbon as carriers and fixed polyaniline within the carbon/polyaniline composites *via in situ* oxidative polymerization. Among them, the negatively charged surface of lignin carbon provides sufficient adsorption sites for positively charged aniline salts (Fig. 11c). Structural analysis indicates that the hierarchically porous carbon offered a large accessible area for the dispersion of aniline, allowing for uniform growth of polyaniline nanofibers. Notably, the layered porous carbon/polyaniline composites exhibited synergistically enhanced electrochemical performance. At a current density of 1.0 A/g, the material demonstrated an exceptional capacitance of 643 F/g. At the same time, the assembled device provided a high energy density of 36.3 Wh/kg at a power density of 850.2 W/kg. Vimala *et al.* [206] synthesized polyaniline-chitosan composites by polymerizing rigid conductive polymer (polyaniline) in an acidic medium. The polymerization of polyaniline molecules in the chitosan matrix led to the expansion of the conjugation effect, thereby improving the charge capacitance. The charge-discharge curves of the composites exhibited double-layer capacitive behavior, with a specific capacitance of 426 F/g. Furthermore, the material demonstrated high cycling stability and a 74 % capacitance retention rate after 500 cycles.

In addition, metal oxides can be combined with biomass-based polymers to fabricate electrodes for SCs. Among them, manganese dioxide (MnO_2) has emerged as one of the most promising *pseudocapacitive* materials due to its high theoretical specific capacitance, abundant availability, simple preparation process, and environmental friendliness. When the carbon material is combined with MnO_2, the two complement each other and produce a synergistic effect, and the natural pore structure of the biomass-based polymer provides favorable conditions for the attachment of MnO_2. Wang *et al.* [207] cultivated salvinia adnata in Hoagland nutrient solution and obtained MnO decorated porous carbon materials (Fig. 11d). The obtained carbon materials not only exhibited layered porous characteristics but also generated *pseudocapacitance* through the redox reactions of manganese oxides. Due to the synergistic effect of the electric double layer and the pseudocapacitance, the composite obtained a high specific capacitance of 436.8 F/g at a current den-

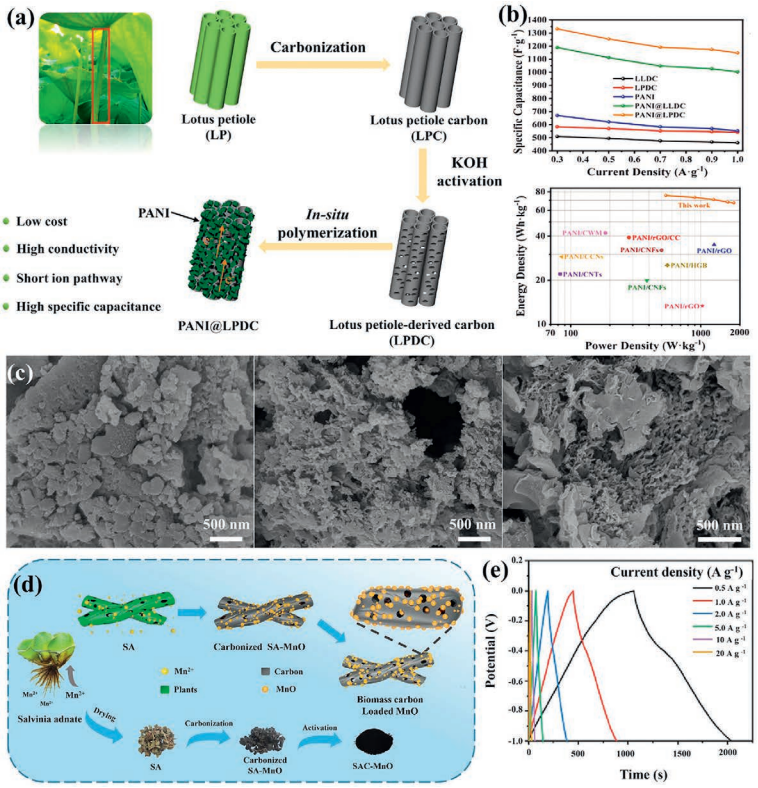


Fig. 11. Copolymerization. (a) Schematic diagram of the preparation of polyaniline@lotus leaf stem-derived carbon composite material. (b) Specific capacitances at different current densities and comparison of the Ragone plots of the present and previously reported devices. Reproduced with permission [204]. Copyright 2024, Elsevier Ltd. (c) SEM images of lignin-derived porous carbon/polyaniline. Reproduced with permission [205]. Copyright 2022, Elsevier Inc. (d) Schematic diagram of the preparation process of MnO-decorated porous carbon. (e) GCD curves at different current densities. Reproduced with permission [207]. Copyright 2023, Elsevier B.V.

sity of 1 A/g, and had an ultra-high specific surface area of 2396 m^2/g and a superior pore volume of 1.538 cm^3/g (Fig. 11e). Zhao *et al.* [208] adopted a simple hydrothermal method to polymerize highly conductive carbon materials derived from pomelo peels with MnO_2, resulting in a composite material resembling the shape of a sea urchin. MnO_2 was densely distributed on the surface of the derived carbon materials, which may be due to the fact that the loose porous carbon materials provide abundant sites for manganese oxides. Such a composite material also achieved the anticipated electrochemical performance for the electrode materials. At a charge-discharge current density of 0.5 A/g, the specific capacitance of the composite electrode reached 205.5 F/g.

4.3. Nanocomposites

In recent years, with the rapid development of nanofabrication technology and nanomaterials, the study of biomass-based polymer resources and their composites with nanomaterials has emerged as a hot research area. Especially in the field of energy storage, biomass-based polymers have attracted more and more attention. The interaction between nanofillers and the polymer matrix highly depends on the design of the system, which greatly affects the dispersion state of the nanoparticles and the performance of the polymer nanocomposites. Therefore, it is crucial to develop reliable methods that can stabilize the dispersion state of nanoparticles within the polymer matrix [209–213]. To this end, researchers are not only committed to improving the internal relationship between different parts, but also hope to further improve the performance of the material through the synergy between the components. These efforts aim to advance the performance of applications such as capacitors and to expand the potential applications of biomass-based polymers.

Zero-dimensional nanofillers usually refer to small spherical nanoparticles or quantum dots with high surface area, which can enhance the interaction with surrounding materials, thereby improving charge storage and capacitance. The advantage of using carbon dots as nano-fillers lies in their ease of dispersion, which can lead to a more uniform morphology. Among them, carbon quantum dots are quite common. Due to their small size, uniform distribution, rich functional groups, and low cost, carbon quantum dots possess potential applications in fields such as fluorescence detection, catalysis, and energy storage. In addition, carbon quantum dots contain a large number of negatively charged oxygen groups, which can improve the wettability of the composites. Furthermore, carbon quantum dots can be regarded as electron donors, and their abundant Π electron clouds can facilitate electron transfer with porous carbon materials, thereby forming electron-rich regions that further enhance the electronic conductivity of the electrode materials. Jin *et al.* [214] developed a simple and effective strategy to prepare biomass-based polymer-derived porous carbon materials. By introducing carbon quantum dots as a functional component into biomass-derived nanofibers, the inherent structural defects of lignin were optimized (Fig. 12a). The introduction of carbon quantum dots effectively reduces the interaction between lignin macromolecules, thereby increasing the flexibility between macromolecular segments. The resulting porous carbon materials not only exhibited high graphitization but also contained a large number of active functional groups on the material's surface, enhancing the energy storage performance. This material displayed a specific capacitance of 294.4 F/g, with a power density of 640 W/kg and an energy density of 28.3 Wh/kg. Quan *et al.* [215] employed a simple strategy to improve the capacitive behavior of porous carbon scaffolds derived from camellia seed shells by introducing carbon quantum dots. The results

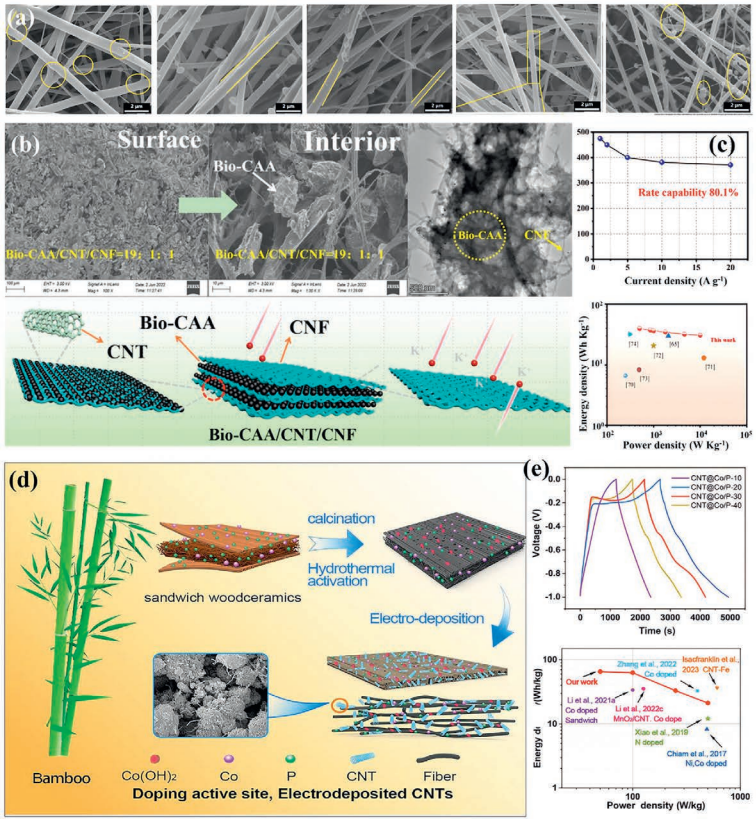


Fig. 12. Zero-dimensional and one-dimensional nanomaterials enhance the performance of supercapacitors. (a) SEM images of biomass-based carbon fibers prepared from carbon quantum dots. Reproduced with permission [214]. Copyright 2024, Elsevier B.V. (b) Schematic diagram of the composite structure and SEM, TEM images. (c) Specific capacitance curve and Ragone plots of the porous carbon and performance comparison with the reported carbon materials. Reproduced with permission [218]. Copyright 2024, Elsevier B.V. (d) Schematic diagram of the synthesis of CNT/Co-porous carbon. (e) GCD curves and energy and power densities. Reproduced with permission [220]. Copyright 2024, Elsevier Ltd.

indicated that the addition of carbon quantum dots made the surface of the layered porous carbon materials rougher, exhibiting a loose sponge-like structure with interconnected three-dimensional open pores. These pores improve the accessibility of active sites, providing short ion transport and accelerating electrolyte diffusion. In addition, the optimized composite material has improved charge/ion transfer kinetics. At a current density of 1 A/g, the capacitance reached 259 F/g. The assembled symmetric SCs exhibited excellent long-term stability, with a capacitance retention of 94 % after 20,000 cycles at 5 A/g. Bu *et al.* [216] prepared porous carbon spheres derived from biomass-based polymers by carbonization and acid etching of sodium alginate. N-doped graphene quantum dots were uniformly grown on the surface of porous carbon spheres, which significantly improved the pseudocapacitive activity and conductivity of porous carbon spheres. The introduction of N-doped graphene quantum dots into the porous carbon sphere structure improved the material's wettability and conductivity, resulting in excellent electrochemical performance. Consequently, the fabricated electrode materials demonstrated a high capacitance of 419.3 F/g, with a maximum energy density of 11.72 Wh/kg and a maximum power density of 12.5 kW/kg.

Compared to zero-dimensional nanomaterials, one-dimensional nanofillers have extended axial dimensions in one direction, such as nanowires, nanofibers, or nanotubes. Studies have shown that one-dimensional filled nanocomposites exhibit the highest polarizability. In these materials, carbon nanotubes can be combined with biomass-based polymer-derived carbon to form flexible electrode composites. In addition, carbon nanotubes can also act as a conductive "vein" to quickly transport charges, enhance the accessibility of electrolyte ions into the electrode material, and buffer the mechanical stress during transport. Rey-Raap *et al.* [217] prepared glucose-derived carbon from glucose as a precursor through hydrothermal carbonization in the presence of multi-walled carbon nanotubes. They determined the optimal dosage for maximizing performance in SCs by adjusting the ratio of carbon nanotubes added during the hydrothermal polymerization of glucose. The results show that the specific capacitance of the electrode material is 206 F/g by adding 2 wt% carbon nanotubes and subsequent chemical activation, and it can still maintain 97 % capacitance after 5000 cycles. Lv *et al.* [218] prepared derived porous carbon aerogels using pineapple leaf fibers and incorporated carbon nanotubes as conductive additives, forming a robust 3D framework with cellulose nanofibers from pineapple leaves (Fig. 12b). The porous structure of the derived porous carbon aerogel can effectively reduce the aggregation of carbon nanotubes, thereby significantly improving the electrochemical performance of the electrode material. Furthermore, the obtained composites exhibited a capacitance of 481 F/g at a current density of 1 A/g and achieved an energy density of 39.63 Wh/kg at a power density of 500 W/kg (Fig. 12c). It is worth noting that the material is light in weight, robust and durable, and can bend arbitrarily and restore its original shape. Thillaikkarasi *et al.* [219] prepared porous carbon derived from the shells of Pongamia pinnata by chemical activation, and prepared electric double layer capacitors with multi-walled carbon nanotubes. The specific surface areas of the prepared porous carbon material and multi-walled carbon nanotubes were 1170 m^2/g and 216 m^2/g, respectively. The carbon composite exhibits excellent electrochemical properties. In a voltage window of 0 to 1.8 V,

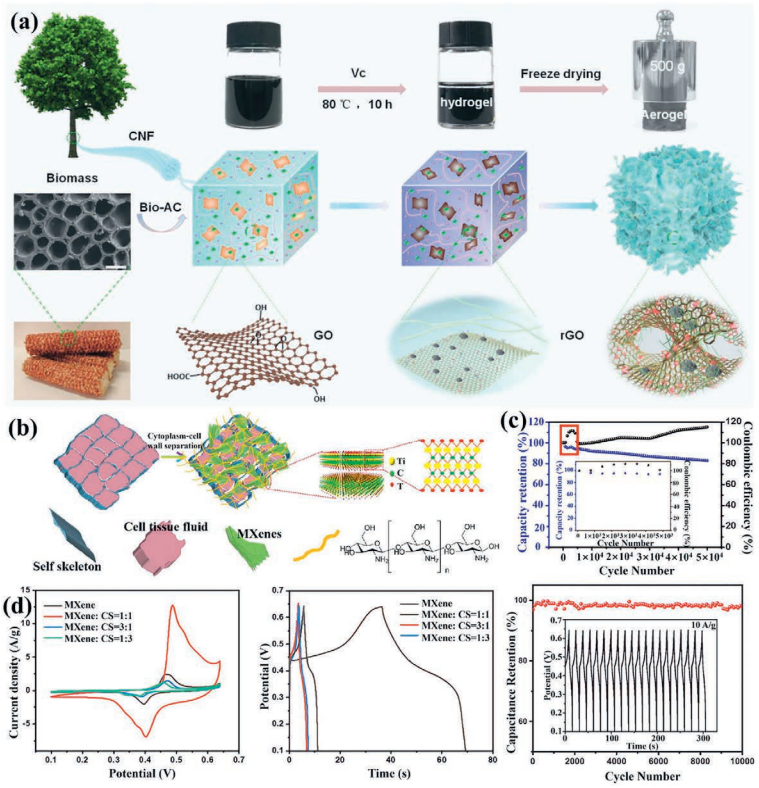


Fig. 13. The enhancement of supercapacitor performance through two-dimensional nanomaterials and metal materials. (a) Schematic diagram of the self-assembly of ternary biomass-based polymer/graphene/nanocellulose aerogels. Reproduced with permission [221]. Copyright 2021, Published by Elsevier B.V. (b) The dispersion mechanism of MXene in radish cells. (c) Curves of the Capacitance retention and Coulombic efficiency with the number of cycles. Reproduced with permission [224]. Copyright 2023, Elsevier B.V. (d) Electrochemical properties of two-dimensional nanomaterials MXene/chitosan. Reproduced with permission [225]. Copyright 2024, Springer Nature.

it exhibited a specific capacitance of 55.51 F/g, an energy density of 4.852 Wh/kg, and a power density of 199.18 W/kg at a current density of 1 A/g. Gong *et al.* [220] used bamboo veneer and bamboo fibers as raw materials to prepare a bamboo-based sandwich structure matrix through acid pretreatment and Co^{2+} catalyzed graphitization method (Fig. 12d). Carbon nanotubes were assembled into the pores through electrodialysis to modulate the pore structure. The results showed that by adding 1wt% multi-walled nanotubes as a deposition electrolyte, the specific capacitance of the electrode material reached up to 453.72 F/g when deposited for 20 min at a current density of 0.2 A/g at room temperature. When the power density is 500 W/kg, the energy density can reach 21.3 Wh/kg (Fig. 12e).

Two-dimensional nanofillers have two longitudinal dimensions, forming a flat or thin sheet structure. Common two-dimensional nanofillers include graphene oxide, reduced graphene oxide and MXene. One advantage of high-dimensional nanofillers is that they can achieve good arrangement, which has a significant effect on the dielectric properties of composites. Among them, graphene has attracted considerable attention as an energy storage material due to its excellent conductivity, large surface area, and thermal stability. With optimal spacing between graphene nanosheets, the high diffusion of electrolyte ions enables a high specific capacitance. Chen *et al.* [221] synthesized carbon/reduced graphene oxide/cellulose nanofiber composite aerogels through a one-step self-assembly method (Fig. 13a). Due to this synergistic effect, the areal capacitance of the composite electrode was significantly enhanced, reaching 1625 mF/cm^2. In addition, a self-supporting SCs was successfully prepared by using a mixed aerogel with a layered structure as an electrode, and a satisfactory capacitance performance was obtained, reaching 4.8 F/cm^2. Xu *et al.* [222] successfully prepared porous carbon derived from Ganoderma lucidum waste combined with graphene composite aerogels through a simple self-assembly method. The addition of graphene can regulate the pore structure and pore size, and significantly improve the conductivity and effective specific surface area of biomass-based polymer-derived porous carbon. When used as an electrode material for SCs, the advantages of the three-dimensional graphene network combined with porous carbon facilitate rapid charge transfer. The resulting composite carbon material exhibits excellent electrochemical performance, achieving a specific capacitance of 176 F/g at a current density of 20 A/g. After 10,000 cycles, the capacitance retention rate reached up to 99.9 %. Guardia *et al.* [223] improved the microporous carbon prepared by one-pot activation of grape seeds by combining reduced graphene oxide. The highly porous carbon particles obtained *via* KOH activation, when mixed with reduced graphene oxide, maintained a high capacitance of 260 F/g in H_2SO_4 aqueous solution at a standard current density of 1 mA/cm^2. In addition, at high current density, the energy stored in the capacitors assembled by these composites increased by 8 times, and the power density increased by 4 times.

MXenes belong to the family of transition metal carbides, nitrides, and carbonitrides, and they are formed by selectively etching the "A" layer of the MAX phase. The etching solution contains fluoride ions such as hydrofluoric acid, ammonium difluoride, hydrochloric acid or lithium fluoride. The two-dimensional materials formed by selectively etching the A layer from the MAX phase are referred to as MXenes, highlighting their graphene-like morphology. Cui *et al.* [224] prepared MXene/chitosan composite aerogels *in situ* using the hydrothermal method (Fig. 13b). In this electrode, the concentration gradient between MXene nanosheets and the radish cells drives the permeation process, with MXene nanosheets embedded within the radish cells. Due to the re-stacking of two-dimensional nanosheets, the electrode made of layered materials

may affect the surface area in contact with the electrolyte. Notably, the assembled binder-free asymmetric SCs exhibited an ultra-high volumetric energy density of 33.4 Wh/L at a high current density of 10 mA/cm^3, while maintaining 82 % of the capacitance rate after 50,000 cycles (Fig. 13c). Pu *et al.* [225] prepared MXene nanocomposite carbon materials by a simple and environmentally friendly method using chitosan as raw material. The resulting carbon composite materials achieved a specific capacitance of up to 286.28 F/g, and after 10,000 charge-discharge cycles, the efficiency remained above 98 % (Fig. 13d). In addition, metal nanoparticles, especially copper, can effectively improve the conductivity and electrochemical activity of electrode materials by embedding metal nanoparticles into porous carbon matrix. Luo *et al.* [226] used Lewis acid as structure protectants, activators, and active materials to prepare standalone hybrid electrodes through a one-step method. In addition, Cu-related particles can provide pseudocapacitance as active substances, providing a fast transport route for redox reactions. Benefiting from the synergistic effect of porous structure and Lewis's acid, the selected lignocellulosic carbon material exhibits excellent performance in SCs. A high capacity value of 451 F/cm^3 was obtained at 400 mA/cm^3, while the energy density reached 25.19 Wh/L at 0.12 W/L. Xi *et al.* [227] prepared porous carbon synthesized by chitosan and Cu nanoparticles. At an activation temperature of 700 °C, the composite achieved a capacitance of 2479 F/g at a current density of 0.5 A/g, exhibiting good cycling stability. After 10,000 charge-discharge cycles, the capacitance retention rate remained at 82.43 %.

Nanofillers of different dimensions possess unique properties and can achieve uniform dispersion within polymer matrices. The synergistic effect between these materials and biomass-based polymer-derived porous carbon helps to improve the electrochemical performance of energy storage devices, including rate performance, power density, energy density and cycle life.

5. Conclusions and perspectives

This review comprehensively summarizes the latest progress of biomass-based polymer-derived porous carbon as electrode materials. Among various electrochemical energy storage technologies, SCs offer unique advantages over typical batteries such as potassium-ion batteries, lithium-ion batteries, and sodium-ion batteries, including long cycle life, fast charge-discharge rates, high power density, and environmental friendliness. In addition, using biomass-derived polymer-based porous carbon as electrode materials not only reduces costs but also conserves resources and minimizes environmental impact. Furthermore, flexible devices using biomass-based polymer-derived porous carbon as electrode materials have been widely used in the field of portable and wearable devices, further expanding the practicality of SCs.

Biomass-based polymers come in various types, each exhibiting different physicochemical properties, making them suitable for a range of applications, particularly in SCs. Natural-based polymers contain a large number of organic compounds and carbon elements. These components provide carbon skeletons during carbonization, which in turn determines the microstructure and basic properties of carbon materials. At the same time, the presence of heteroatoms can also facilitate electrochemical performance to some extent. Biomass-based polymers that are converted from low molecules to polymers form complex polymer structures through the polymerization of low-molecular monomers. Furthermore, these synthesized high molecular weight biomass-based polymers not only possess high specific surface area and excellent electrical conductivity but also exhibit good mechanical properties and thermal conductivity, among other attributes.

There is a complex relationship between the energy storage characteristics of electrochemical energy storage devices and their pore structures. Therefore, researchers have adopted various strategies to prepare derived carbon with ideal porous structure. Techniques such as pyrolysis, hydrothermal carbonization, acid activation, alkali activation, and salt activation have been widely used to produce derived carbons with controllable pore size distribution and large specific surface areas. Pyrolysis and carbonization are the primary steps in the preparation of derived porous carbon. The properties of biomass-based polymer-derived porous carbon are often influenced by factors such as pyrolysis temperature, heating rate, and residence time. Physical activation involves the oxidation reaction of C, and further reaction of the activator with C to obtain a well-developed pore structure. In contrast, chemical activation employs activating agents such as H_3PO_4, KOH, and $ZnCl_2$ to react with carbon materials, typically resulting in porous carbon with high product yield and large specific surface area.

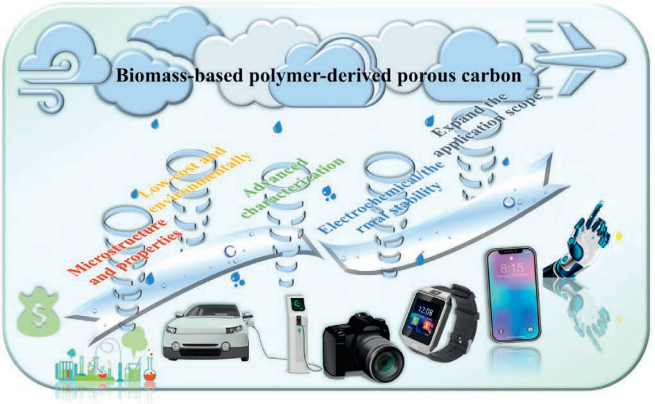


Fig. 14. Looking ahead to the potential research directions for the future development of biomass-based polymer-derived porous carbon materials.

In addition to the above methods, high-performance carbon materials also need to explore some new methods to modify carbon materials. Introducing heteroatoms (such as N, P, S, O, B) as electron donors or acceptors is an effective method that can significantly enhance the electrochemical performance of biomass-based polymer-derived carbon. The variation in electronegativity among the doped atoms can lead to different interactions between ions and carbon. The introduced polymers not only enhance conductivity but can also increase the capacity of the electrode through additional Faradaic redox reactions, thereby achieving pseudocapacitance effects. In addition, the addition of nano-fillers can form a multi-component, multi-level structure of the composite material, and the synergy between the components can give the composite material more unexpected performance, such as improving the electrochemical performance.

Although biomass-based polymer-derived porous carbon exhibits significant potential in SCs, there are still many limiting factors that pose considerable challenges to its development, necessitating further exploration (Fig. 14).

(1) There is a lack of comprehensive understanding of the microstructure and properties of biomass-based polymers. Therefore, further research is necessary to understand the modulation of pore properties and their impact on electrochemical performance. Because in the process of electrochemical reaction, it is very important to study the transport or storage of ions in different pore structures. The development of more complex characterization methods, along with a thorough understanding and analysis of the structural and electrochemical properties, is essential. Moreover, theoretical calculations also play a key role in revealing the microstruc-

ture, degree of polymerization and dynamic changes of derived porous carbon.

(2) Developing low-cost, scalable, and environmentally friendly production processes for the extraction of biomass-based polymers and the preparation of derived porous carbons is an urgent need for their commercial application. In the process of converting biomass-based polymers into carbon materials, the chemicals used and the heat treatment involved are expensive. For example, the extraction of chitosan requires high temperature treatment with strong acid and alkali, which will produce a large amount of wastewater and energy consumption, and it is difficult to achieve large-scale production.

(3) When incorporating nanofillers, it is necessary to conduct a series of advanced characterizations of the nanostructures, including the shape, size, and location of the pores, interlayer spacing, and specific surface area. This information will assist us in achieving the bottom-up design of biomass-based polymer-derived porous carbon, thereby endowing it with an ideal microstructure and specific application performance.

(4) The electrochemical/thermal stability of SCs should be improved. A rational design of the polymer matrix and electrolyte can further enhance thermal stability and extend the electrochemical stability window. A rational design of the polymer matrix and electrolyte can further enhance thermal stability and extend the electrochemical stability window.

(5) Combining biomass-based polymer-derived porous carbon with advanced technologies in other fields can significantly expand its application range. For example, energy storage devices suitable for implantation in the human body can be designed while maintaining the biocompatibility advantages of biomass-based polymers as biomedical devices. In addition, it can also be applied to flexible electronic devices to develop fully flexible self-powered devices with high power density and energy density. The development of devices with new functions (such as self-healing, temperature sensitivity, and electrochromism) is critical to further expand their application in the next generation of intelligent electronic devices.

Declaration of competing interest

The authors declare that they have no known competing financial interests or personal relationships that could have appeared to influence the work reported in this paper.

CRediT authorship contribution statement

Qiqi Lv: Writing – original draft. **Zhiwei Tian:** Writing – review & editing. **Weijun Li:** Supervision. **Gaigai Duan:** Conceptualization. **Xiaoshuai Han:** Conceptualization. **Chunmei Zhang:** Conceptualization. **Shuijian He:** Methodology. **Haimei Mao:** Conceptualization. **Chunxin Ma:** Supervision. **Shaohua Jiang:** Writing – review & editing.

References

[1] Y. Liu, L.J. Wu, Nano Energy 109 (2023) 108290.
[2] Y.P. Ma, C.X. Hou, H. Kimura, et al., Adv. Compos. Hybrid Mater. 6 (2023) 59.
[3] L.J. Xie, C. Tang, M.X. Song, et al., J. Energy Chem. 72 (2022) 554–569.
[4] C. Liu, T. Lei, F. Seidi, et al., Energy Storage Mater. 72 (2024) 103774.
[5] Y. Wang, T. Xu, K. Liu, et al., Aggregate 5 (2023) e428.
[6] W.J. Lu, Y.X. Si, C.R. Zhao, et al., Chem. Eng. J. 495 (2024) 153311.
[7] Z.K. Chen, X.L. Jiang, Y. Boyjoo, et al., Electrochem. Energy R 7 (2024) 26.
[8] Z.Y. Zhu, Y. Men, W.J. Zhang, et al., eScience 4 (2024) 100249.
[9] N.S. George, G. Singh, R. Bahadur, et al., Adv. Sci. 11 (2024) 2406235.
[10] L. Li, J. Yang, G. Duan, et al., J. Energy Storage 90 (2024) 111933.
[11] Y.Z. Huang, L. Xing, S. Pei, et al., Trans. Noneferr. Met. Soc. 33 (2023) 3452–3464.
[12] Y. Liu, K. Xiang, W. Zhou, et al., Small 20 (2023) 2308741.
[13] L. Li, J.S. Nam, M.S. Kim, et al., Adv. Energy Mater. 13 (2023) 2302139.
[14] F. Xiankai, X. Kaixiong, Z. Wei, et al., Carbon Energy 6 (2024) e536.
[15] S.T. Jiang, J. Fang, H.Y. Liu, et al., Chem. Eng. J. 502 (2024) 157745.
[16] Z.X. Guo, Z.W. Tian, G.G. Duan, et al., Chem. Eng. J. 501 (2024) 157702.
[17] Z.W. Tian, C. Yang, C.M. Zhang, et al., J. Energy Storage 85 (2024) 111130.
[18] Y. Shao, F. Shen, Y. Shao, ChemElectroChem 8 (2020) 484–491.
[19] G. Pacchioni, Nat. Rev. Mater. 7 (2022) 844.
[20] P. Simon, Y. Gogotsi, Nat. Mater. 19 (2020) 1151–1163.
[21] Y. Zhou, H.L. Qi, J.Y. Yang, et al., Energy Environ. Sci. 14 (2021) 1854–1896.
[22] Z. Shang, X. An, S. Nie, et al., J. Bioresour. Bioprod. 8 (2023) 292–305.
[23] S. Jiang, M. Xie, L. Jin, et al., Chin. Chem. Lett. 36 (2025) 110293.
[24] M.H. Li, L. Bai, S.T. Jiang, et al., J. Hazard. Mater. 452 (2023) 131352.
[25] M.S.M. Zaini, M. Arshad, S.S.A. Syed-Hassan, J. Bioresour. Bioprod. 8 (2023) 66–77.
[26] H.S. Shahraki, R. Bushra, N. Shakeel, et al., J. Bioresour. Bioprod. 8 (2023) 162–175.
[27] X. Chen, Q. Tang, L. Chang, et al., J. For. Eng. 8 (2023) 110–120.
[28] J. Wang, P. Nie, B. Ding, et al., J. Mater. Chem. A 5 (2017) 2411–2428.
[29] W. Yang, W. Yang, J. Zeng, et al., Prog. Mater. Sci. 144 (2024) 101264.
[30] S. Dalwadi, A. Goel, C. Kapetanakis, et al., Int. J. Mol. Sci. 24 (2023) 3975.
[31] Y.F. Yin, Q.J. Liu, Y.T. Zhao, et al., Energy Fuels 37 (2023) 3523–3554.
[32] X.F. Tang, D. Liu, Y.J. Wang, et al., Prog. Mater. Sci. 118 (2021) 100770.
[33] C. Chen, L. Hu, Acc. Chem. Res. 51 (2018) 3154–3165.
[34] H. Zhu, W. Luo, P.N. Ciesielski, et al., Chem. Rev. 116 (2016) 9305–9374.
[35] F. Jiang, T. Li, Y.J. Li, et al., Adv. Mater. 30 (2018) 1703453.
[36] J. Mazurkiewicz, Energies 15 (2022) 413.
[37] B. Chen, J.A. Koziel, A. Bialowiec, et al., J. Environ. Manag. 370 (2024) 122692.
[38] Y.C. Huang, Z. Tang, S.Y. Zhou, et al., J. Phys. D Appl. Phys. 55 (2022) 313002.
[39] W. Tong, X. Liang, X. Zhou, et al., J. For. Eng. 9 (2024) 77–83.
[40] Y. Zhang, Y. Zhao, Y. Wu, et al., Int. J. Biol. Macromol. 214 (2022) 414–425.
[41] S. Abang, F. Wong, R. Sarbatly, et al., J. Bioresour. Bioprod. 8 (2023) 361–387.
[42] F. Fahma, N. Lisdayana, Z. Abidin, et al., J. Polym. Environ. 111 (2020) 1354–1363.
[43] H.W. Kwak, H. Lee, M.E. Lee, et al., J. Clean. Prod. 200 (2018) 1034–1042.
[44] W. Zhu, Y. Zhang, X.Y. Wang, et al., Cellulose 29 (2022) 817–833.
[45] N. Zainuddin, I. Ahmad, H. Kargarzadeh, et al., Carbohydr. Polym. 163 (2017) 261–269.
[46] M. Mujtaba, A.M. Salaberria, M.A. Andres, et al., Int. J. Biol. Macromol. 104 (2017) 944–952.
[47] H. Jin, T. Zhang, Z. Tian, et al., J. For. Eng. 9 (2024) 103–109.
[48] Q. Fu, Y.H. Liu, T. Liu, et al., Nano Energy 102 (2022) 107739.
[49] Z.T. Wei, J.L. Wang, Y.H. Liu, et al., Adv. Funct. Mater. 32 (2022) 2208277.
[50] K. Shi, H. Zou, B. Sun, et al., Adv. Funct. Mater. 30 (2019) 1904536.
[51] Q.L. Qu, X.L. Zhang, J. Muhire, et al., Colloids Surf. B: Biointerfaces 244 (2024) 114184.
[52] C.Q. You, L.K. Ning, Z. Zhang, et al., Carbohydr. Polym. 289 (2022) 119432.
[53] K.J. Nagarajan, N.R. Ramanujam, M.R. Sanjay, et al., Polym. Compos. 42 (2021) 1588–1630.
[54] H. Yang, Y. Zhang, R. Kato, et al., Carbohydr. Polym. 212 (2019) 30–39.
[55] A. Ozen, A. Karabiber, S. Sener, et al., Phys. Status Solidi (A) 220 (2023) 2300191.
[56] M.K.M. Haafiz, S.J. Eichhorn, A. Hassan, et al., Carbohydr. Polym. 93 (2013) 628–634.
[57] A.B. Perumal, R.B. Nambiar, J.A. Moses, et al., Food Hydrocoll. 127 (2022) 107484.
[58] J.J. Yang, X.S. Han, W.S. Yang, et al., Environ. Res. 236 (2023) 116736.
[59] S. Zhou, X. Kong, B. Zheng, et al., ACS Nano 13 (2019) 9578–9586.
[60] S.W. Kim, K.H. Lee, Y.H. Lee, et al., Adv. Sci. 9 (2022) 2203720.
[61] H. Lai, Z. Chen, H. Zhuo, et al., Chin. Chem. Lett. 35 (2024) 108331.
[62] L.J. Andrew, E.R. Gillman, C.M. Walters, et al., Small 19 (2023) 2301947.
[63] Q.Q. Lv, X.F. Ma, C.M. Zhang, et al., Int. J. Biol. Macromol. 259 (2024) 129268.
[64] S.N. Fernandes, P.L. Almeida, N. Monge, et al., Adv. Mater. 29 (2017) 1603560.
[65] N.H. Avcioglu, World J. Microbiol. Biotechnol. 38 (2022) 86.
[66] S.J. Wang, C.L. Li, L. Copeland, et al., Compr. Rev. Food Sci. Food Saf. 14 (2015) 568–585.
[67] G. Scott, J.M. Awika, Compr. Rev. Food Sci. Food Saf. 22 (2023) 2081–2111.
[68] T.J. Gutiérrez, J. Tovar, Trends Food Sci. Technol. 109 (2021) 711–724.
[69] J.C. Tu, B. Adhikari, M.A. Brennan, et al., Food Hydrocoll. 139 (2023) 108504.
[70] L.Y. Wang, M. Wang, Y.H. Zhou, et al., Food Chem. 377 (2022) 131990.
[71] Z.Y. Wang, P. Mhaske, A. Farahnaky, et al., Food Hydrocoll. 129 (2022) 107542.
[72] Q. Liu, L. Gao, Y. Qin, et al., Food Packag. Shelf Life 35 (2023) 101032.
[73] R.F. Tester, J. Karkalas, X. Qi, J. Cereal Sci. 39 (2004) 151–165.
[74] Q.T. Luo, T.P. Zeng, K. Gu, et al., ACS Appl. Energy Mater. 7 (2024) 11610–11632.
[75] X.G. Dang, N. Li, Z.F. Yu, et al., Carbohydr. Polym. 342 (2024) 122385.
[76] J.L. Espinoza-Acosta, P.I. Torres-Chávez, J.L. Olmedo-Martínez, et al., J. Energy Chem. 27 (2018) 1422–1438.
[77] W.L. Zhang, J. Yin, C.W. Wang, et al., Small Methods 5 (2021) 2100896.
[78] R. Madhu, A.P. Periasamy, P. Schlee, et al., Carbon 207 (2023) 172–197.
[79] X.R. Yang, Y.F. Zhang, M.H. Ye, et al., Green Chem. 25 (2023) 4154–4179.
[80] Y.Y. Fan, C. Liu, X.C. Kong, et al., Green Energy Environ. 7 (2022) 1318–1326.
[81] M. Xu, X. Zhu, Y. Lai, et al., Appl. Energy 353 (2024) 122095.
[82] C.X. Huang, Z.W. Peng, J.J. Li, et al., Ind. Crops Prod. 187 (2022) 115388.

[83] R.R. Singhania, A.K. Patel, T. Raj, et al., Fuel 311 (2022) 122608.
[84] A.P. Khedulkar, B. Pandit, V.D. Dang, et al., Sci. Total Environ. 869 (2023) 161441.
[85] D. Dong, Y. Xiao, Chem. Eng. J. 470 (2023) 144441.
[86] J. Wei, F. Hu, Y. Pan, et al., Chem. Eng. J. 481 (2024) 148793.
[87] J.K. Sahoo, O. Hasturk, T. Falcucci, et al., Nat. Rev. Chem. 7 (2023) 302–318.
[88] H.Y. Zheng, B.Q. Zuo, J. Mater. Chem. B 9 (2021) 1238–1258.
[89] C. Holland, K. Numata, J. Rnjak-Kovacina, et al., Adv. Healthc. Mater. 8 (2019) 1800465.
[90] J. Li, S. Li, J. Huang, et al., Adv. Sci. 9 (2021) 2103965.
[91] W.C. Lu, C.S. Chiu, Y.J. Chan, et al., Aquac. Rep. 29 (2023) 101514.
[92] Y. Zhang, Y. Wang, Y. Li, et al., Gels 9 (2023) 185.
[93] Z. Rajabimashhadi, N. Gallo, L. Salvatore, et al., Polymers 15 (2023) 544 Basel.
[94] S. Gaikwad, M.J. Kim, Mar. Drugs 22 (2024) 60.
[95] J. Zhu, N. Ma, S. Li, et al., Adv. Funct. Mater. 33 (2023) 2213644.
[96] K.G. Motora, C.M. Wu, C.R.M. Jose, et al., Adv. Funct. Mater. 34 (2024) 2315069.
[97] L.K. Sellappan, S. Manoharan, Int. J. Biol. Macromol. 259 (2024) 129162.
[98] C.R. Chilakamarry, S. Mahmood, S.N.B.M. Saffe, et al., 3 Biotech 11 (2021) 220.
[99] X. Zhang, Q. Qu, A. Yang, et al., Carbohydr. Polym. 299 (2023) 120134.
[100] Q.L. Qu, A.Q. Yang, J. Wang, et al., J. Colloid Interface Sci. 649 (2023) 68–75.
[101] M. Luo, Z.Q. Zhu, K. Yang, et al., Sci. Total Environ. 747 (2020) 141923.
[102] Q. Wu, J.Q. Hu, S.S. Cao, et al., Int. J. Biol. Macromol. 155 (2020) 131–141.
[103] S. Rahman, J. Gogoi, S. Dubey, et al., Int. J. Biol. Macromol. 255 (2024) 128197.
[104] M.C.E. Lomer, Proc. Nutr. Soc. 83 (2023) 17–27.
[105] X. Chen, R. Wang, Z. Tan, Food Chem. 412 (2023) 135557.
[106] S.X. Su, P.P. Long, Q. Zhang, et al., Food Chem. 446 (2024) 138827.
[107] M. Zhang, C. Tang, Z.C. Wang, et al., Nat. Methods 21 (2024) 609–618.
[108] Z.N. Ling, Y.F. Jiang, J.N. Ru, et al., Signal Transduct. Target. Ther. 8 (2023) 345.
[109] J. Thomas, R. Patil, Ind. Eng. Chem. Res. 62 (2023) 1725–1735.
[110] H.H. Wang, Z.Y. Huang, X.L. Zeng, et al., ACS Appl. Electron. Mater. 5 (2023) 3726–3732.
[111] X.Y. Lu, X.L. Gu, Int. J. Biol. Macromol. 229 (2023) 778–790.
[112] M.Y. Zhi, X. Yang, R. Fan, et al., Polym. Degrad. Stab. 201 (2022) 109976.
[113] Z. Chen, X. Liu, H. Chen, et al., Chin. Chem. Lett. 35 (2024) 109194.
[114] X.Q. Mi, N. Liang, H.F. Xu, et al., Prog. Mater. Sci. 130 (2022) 100977.
[115] W. Li, G.H. Wang, W.J. Sui, et al., Carbon 196 (2022) 819–827.
[116] X.Y. Wang, X.W. Yang, C. Zhao, et al., Angew. Chem. Int. Ed. 62 (2023) e202302829.
[117] Z. Peng, X. Jiang, C. Si, et al., ChemSusChem 16 (2023) e202300174.
[118] A. Zapaśnik, B. Sokołowska, M. Bryła, Foods 11 (2022) 1283.
[119] A. Vlachopoulos, G. Karlioti, E. Balla, et al., Pharmaceutics 14 (2022) 359.
[120] T.A. Swetha, V. Ananthi, A. Bora, et al., Int. J. Biol. Macromol. 234 (2023) 123703.
[121] W.W. Shi, T.J. Cassmann, A.V. Bhagwate, et al., Cell Rep. 43 (2024) 113746.
[122] J. Kang, D. Miyajima, T. Mori, et al., Science 347 (2015) 646–651.
[123] S. Dadashi-Silab, S. Doran, Y. Yagci, Chem. Rev. 116 (2016) 10212–10275.
[124] K.R. Guo, J.R. Wang, Z. Shi, et al., Angew. Chem. Int. Ed. 62 (2023) e202213606.
[125] Z.P. Zhou, L. Zhang, Y.H. Yang, et al., Nat. Chem. 15 (2023) 841.
[126] H.M.T. Choi, V.A. Beck, N.A. Pierce, ACS Nano 8 (2014) 4284–4294.
[127] S.Y. Tao, S.J. Zhu, T.L. Feng, et al., Angew. Chem. Int. Ed. 59 (2020) 9826–9840.
[128] N. Reddy, R. Reddy, Q.R. Jiang, Trends Biotechnol. 33 (2015) 362–369.
[129] A. Oryan, A. Kamali, A. Moshiri, et al., Int. J. Biol. Macromol. 107 (2018) 678–688.
[130] H. Nasution, H. Harahap, N.F. Dalimunthe, et al., Gels 8 (2022) 568.
[131] H.R. Qiang, J.W. Wang, H.X. Liu, et al., Polym. Chem. 14 (2023) 4255–4274 UK.
[132] W. Ali, H. Ali, S. Gillani, et al., Environ. Chem. Lett. 21 (2023) 1761–1786.
[133] G. Li, M.H. Zhao, F. Xu, et al., Molecules 25 (2020) 5023.
[134] M.J. Wang, Q.Q. Li, C.Z. Shi, et al., Nat. Nanotechnol. 18 (2023) 403–411.
[135] M. Koller, A. Mukherjee, Bioengineering 9 (2022) 74 Basel.
[136] A. Dhaini, V. Hardouin-Duparc, A. Alaaeddine, et al., Prog. Polym. Sci. 149 (2024) 101781.
[137] D.M. Lee, N. Rubab, I. Hyun, et al., Sci. Adv. 8 (2022) eabl8423.
[138] L.P. Wang, Y.Z. Chang, A.M. Li, Renew. Sustain. Energy Rev. 108 (2019) 423–440.
[139] H.Z. He, R.Q. Zhang, P.C. Zhang, et al., Adv. Sci. 10 (2023) 2205557.
[140] Z. Xu, J. Wang, Z.Y. Guo, et al., Adv. Energy Mater. 12 (2022) 2200208.
[141] B. Ercan, K. Alper, S. Ucar, et al., J. Energy Inst. 109 (2023) 101298.
[142] S. Wu, Q. Wang, M.H. Fang, et al., Sci. Total Environ. 897 (2023) 165327.
[143] P. Zhang, Y. Chen, X. Song, et al., Chem. Eng. J. 503 (2025) 157703.
[144] H.S. Li, F.Y. Shi, Q.D. An, et al., Int. J. Biol. Macromol. 166 (2021) 923–933.
[145] P. Sangsiri, N. Laosiripojana, P. Daorattanachai, Renew. Energy 193 (2022) 113–127.
[146] Y.D. Chen, F. Liu, N.Q. Ren, et al., Chin. Chem. Lett. 31 (2020) 2591–2602.
[147] Y.L. Zhou, W. Yan, X.Y. Yu, et al., J. Energy Storage 32 (2020) 101706.
[148] E.A. Hirst, A. Taylor, R. Mokaya, J. Mater. Chem. A 6 (2018) 12393–12403.
[149] S. Zhong, L. Dai, H. Xu, et al., Diam. Relat. Mater. 141 (2024) 110714.
[150] Z.X. Guo, X.S. Han, C.M. Zhang, et al., Chin. Chem. Lett. 35 (2024) 109007.
[151] S. Rawat, R.K. Mishra, T. Bhaskar, Chemosphere 286 (2022) 131961.
[152] G. Jiang, R.A. Senthil, Y. Sun, et al., J. Power Sources 520 (2022) 230886.
[153] J.H. Noh, K.Y. Lee, J.H. Kim, et al., Colloids Surf. Physicochem. Eng. Asp. 682 (2024) 132874.
[154] S. Zhang, Y. Yu, M.J. Xie, et al., Appl. Surf. Sci. 589 (2022) 153011.
[155] Y.L. Zhang, W. Sun, F.Q. Yang, J. Energy Storage 37 (2021) 102476.
[156] S.S. Gunasekaran, S. Badhulika, J. Energy Storage 41 (2021) 102997.
[157] S. Rawat, L. Jinlin, A.A. Ambalkar, et al., J. Energy Storage 60 (2023) 106598.
[158] S. Rawat, T. Boobalan, M. Sathish, et al., Biomass Bioenergy 171 (2023) 106747.
[159] L. Yang, X.T. Guo, Z.K. Jin, et al., Nano Today 37 (2021) 101075.
[160] Q.Y. Kong, Q. Zhang, B. Yan, et al., J. Energy Storage 80 (2024) 110322.
[161] J.Y. Hao, B.X. Wang, H. Xu, et al., J. Energy Storage 86 (2024) 111301.
[162] Y. Cheng, M. Chen, K. Xia, et al., J. Power Sources 624 (2024) 235523.
[163] N. Ahmad, A. Rinaldi, M. Sidoli, et al., J. Energy Storage 99 (2024) 113267.
[164] Y. Chen, C. Zhou, X. Xing, et al., Chem. Eng. J. 495 (2024) 153579.
[165] M. Gautam, T. Patodia, K. Sachdev, et al., Biomass Convers. Biorefin. (2024).
[166] M.K. Jha, D. Shah, P. Mulmi, et al., Mater. Lett. 344 (2023) 134436.
[167] H. Liu, F. Zhang, X. Lin, et al., Nanoscale Adv. 5 (2023) 2831.
[168] A. Sandeep, A.V. Ravindra, Diam. Relat. Mater. 146 (2024) 111158.
[169] Y. Xia, H.F. Zuo, J.L. Lv, et al., J. Clean. Prod. 396 (2023) 136517.
[170] S.M. Wu, H. Zhou, Y.H. Zhou, et al., J. Alloys Compd. 859 (2021) 157814.
[171] Y. Sun, Z. He, H. Fan, et al., J. Power Sources 614 (2024) 235027.
[172] F.P. Wang, T. Liao, S.J. Hu, et al., J. Energy Storage 91 (2024) 112081.
[173] Y. Shu, Q.H. Bai, G.X. Fu, et al., Carbohydr. Polym. 227 (2020) 115346.
[174] G.J. Wang, Z.H. Lin, S.H. Jin, et al., J. Energy Storage 45 (2022) 103525.
[175] X. Zheng, Z.L. Lei, J.R. Wang, et al., Biomass Bioenergy 181 (2024) 107063.
[176] H. Luo, R. Si, C. Li, et al., Mater. Chem. Front. 6 (2022) 379–389.
[177] C.W. Li, H.L. Chen, L.Q. Zhang, et al., Polymers 13 (2021) 4463 Basel.
[178] P. Liang, R.C. Zhang, L.K. Ji, et al., J. Energy Storage 97 (2024) 112823.
[179] W.Y. Tang, C.Y. Fu, P. Lyu, et al., Powder Technol. 392 (2021) 38–46.
[180] S. Yang, Y. Cui, G. Yang, et al., J. Power Sources 554 (2023) 232347.
[181] C.N. Feng, H.B. Tang, X.F. Guo, et al., Mater. Chem. Phys. 245 (2020) 122785.
[182] L. Yang, X.J. He, Y.C. Wei, et al., Nano Res. 15 (2022) 4068–4075.
[183] M.B. Arvas, H. Gürsu, M. Gencten, et al., J. Energy Storage 35 (2021) 102328.
[184] T. Wang, D.L. Wu, F. Yuan, et al., Chem. Eng. J. 462 (2023) 142292.
[185] F.T. Ran, X.B. Yang, X.Q. Xu, et al., Chem. Eng. J. 412 (2021) 128673.
[186] Y. Hu, C. Tang, H.T. Li, et al., Chin. Chem. Lett. 33 (2022) 480–485.
[187] N. Huang, C. Tang, H. Jiang, et al., Nano Res. 17 (2023) 2619–2627.
[188] H.C. Li, J. Zhao, J.H. Liu, et al., Solid State Ion. 414 (2024) 116631.
[189] K.H. Kim, Y.J. Song, H.J. Ahn, Korean J. Chem. Eng. 40 (2023) 1071–1076.
[190] Z. Tian, C. Yang, Z. Guo, et al., Fuels 381 (2025) 133298.
[191] X.Y. Zheng, Y.J. Tao, L.Z. Jin, et al., Ind. Crops Prod. 218 (2024) 119034.
[192] J. Guo, D.L. Wu, T. Wang, et al., Appl. Surf. Sci. 475 (2019) 56–66.
[193] X. Meng, D. Zhang, B. Wang, et al., J. Energy Storage 57 (2023) 106345.
[194] J. Singh, B. Dey, A. Syed, et al., Diam. Relat. Mater. 149 (2024) 111640.
[195] S.Q. Huang, Y. Ding, Y.C. Li, et al., Energy Fuels 35 (2021) 1557–1566.
[196] W.M. Yin, L.F. Tian, B. Pang, et al., Int. J. Biol. Macromol. 156 (2020) 988–996.
[197] P.C. Du, L.H. Liu, Y.W. Dong, et al., Electrochim. Acta 370 (2021) 137801.
[198] Q.Q. Zhou, Q. Chen, W.J. Xu, et al., Chem. Eng. J. 496 (2024) 154126.
[199] Y.J. Li, X.F. Zou, S.Q. Li, et al., J. Mater. Chem. A 12 (2024) 18324–18337.
[200] N.N. Loganathan, V. Perumal, B.R. Pandian, et al., J. Energy Storage 49 (2022) 104149.
[201] S. Sardana, A. Gupta, K. Singh, et al., J. Energy Storage 45 (2022) 103510.
[202] E. Dhandapani, S. Thangarasu, S. Ramesh, et al., J. Energy Storage 52 (2022) 104937.
[203] A. Saeed, S. Khalid, M.N. Anjum, ChemistrySelect 9 (2024) e202303527.
[204] P. Gao, Y.N. Peng, S.Q. Wang, et al., Electrochim. Acta 486 (2024) 144112.
[205] F.B. Fu, H. Wang, D.J. Yang, et al., J. Colloid Interface Sci. 617 (2022) 694–703.
[206] V. Vimala, L. Cindrella, Chem. Phys. Lett. 809 (2022) 140172.
[207] H.T. Wang, H.T. Chen, X. Hou, et al., Diam. Relat. Mater. 136 (2023) 109888.
[208] X.Y. Zhao, N. Wang, L. Li, et al., J. Chem. 2024 (2024) 2779104 Ny.
[209] J. Urzúa, P.S. Poon, J. Matos, J. Non-Cryst. Solids 626 (2024) 122779.
[210] Y.X. Yang, K.K. Ge, S.U. Rehman, et al., Rare Met. 41 (2022) 3957–3975.
[211] B.K. Saikia, S.M. Benoy, M. Bora, et al., Fuel 282 (2020) 118796.
[212] C.Y. Xiong, C.M. Zheng, X. Jiang, et al., J. Energy Storage 72 (2023) 108633.
[213] D.G. Sun, C. Tang, H. Cheng, et al., J. Energy Chem. 72 (2022) 1–8.
[214] Z.X. Jin, Q.P. Cao, H. Gong, et al., J. Power Sources 608 (2024) 234264.
[215] H.Y. Quan, W.H. Tao, Y. Wang, et al., J. Energy Storage 55 (2022) 105573.
[216] J. Bu, Z. Zhou, X. Wu, et al., J. Mater. Sci. 56 (2021) 17694–17708.
[217] N. Rey-Raap, M. Enterría, J.I. Martins, et al., ACS Appl. Mater. Interfaces 11 (2019) 6066–6077.
[218] Y.X. Lv, C.H. Qi, Y.F. Bai, et al., Diam. Relat. Mater. 149 (2024) 111530.
[219] D. Thillaikkarasi, S. Karthikeyan, R. Ramesh, et al., Carbon Lett. 32 (2022) 1481–1505.
[220] L. Gong, R.X. Zeng, Y.Q. Shi, et al., Bioresour. Technol. 399 (2024) 130573.
[221] R.W. Chen, X.S. Li, Q.B. Huang, et al., Chem. Eng. J. 412 (2021) 128755.
[222] M.M. Xu, A.Q. Wang, Y. Xiang, et al., J. Clean. Prod. 315 (2021) 128110.
[223] L. Guardia, L. Suárez, N. Querejeta, et al., Electrochim. Acta 298 (2019) 910–917.
[224] Y.H. Cui, Q.S. Shi, Z. Liu, et al., Chem. Eng. J. 472 (2023) 144701.
[225] L. Pu, J. Zhang, N.K.L. Jiresse, et al., Adv. Compos. Hybrid Mater. 5 (2021) 356–369.
[226] M. Luo, K. Yang, D.T. Zhang, et al., Int. J. Biol. Macromol. 187 (2021) 903–910.
[227] Y.R. Xi, Z.Y. Xiao, H. Lv, et al., J. Colloid Interface Sci. 630 (2023) 525–534.